Electron impact excitation of the electronic states of N_2. I. Differential cross sections at incident energies from 10 to 50 eV‡

D. C. Cartwright
Laboratories Division, The Aerospace Corporation, El Segundo, California 90245
*and Theoretical Division, Los Alamos Scientific Laboratory, Los Alamos, New Mexico 87545**

A. Chutjian, S. Trajmar, and W. Williams
Jet Propulsion Laboratory, California Institute of Technology, Pasadena, California 91103
(Received 11 May 1977)

Normalized differential cross sections (DCS's) for the electron impact excitation of the lowest three singlet (a',a,ω), and lowest five triplet (A,B,W,B',C) valence electronic states of N_2, and of the two ($3s\sigma_g$) Rydberg states (E,a'') have been determined at seven incident electron energies ranging from 10 to 50 eV. These DCS's were obtained for the scattering-angle range 5° to 138° by analyzing electron energy-loss spectra in N_2 at a number of fixed scattering angles within that range. These data, which are the first that cover such a large incident energy and scattering-angle range for such a wide variety of final target states, show that each of the DCS's for the ten final target states falls into one of four classes. Since the initial molecular target state is a singlet, and none of the final states studied here is dipole allowed, these four classes are determined according to whether the final target state is triplet, singlet, parity-unfavored, or Rydberg in character. The DCS's for all the final target states change rapidly in shape as the incident electron energy is varied. Theoretical DCS's obtained from first-order perturbation models (Born-Ochkur and Ochkur-Rudge) agree poorly with the measured DCS's.

I. INTRODUCTION

Differential cross sections (DCS's) for elastic[1] or inelastic electron-atom (molecule) scattering events contain a great deal of information on the physics of the electron-target interaction. For example, individual partial-wave contributions for the elastic scattering process can be obtained from the elastic DCS. For inelastic scattering, quantitative estimates of the contributions from direct, exchange, direct-polarization, etc., excitation mechanisms can similarly (in principle) be determined. Because of this rich information content in the DCS's, one of the best tests for any theoretical description of a scattering process is its ability to reproduce the magnitude and shape of the angular distributions, at all incident particle energies and all scattering angles. In addition to the role of the DCS in providing information on the fundamental physics of the interaction of various particles, it now appears that DCS's for inelastic electron-atom (molecule) processes are also needed (as well as the customary integral cross sections) in order to account properly for the behavior of electrons in gaseous media (e.g., inelastic momentum transfer, etc.).

For electron-atom inelastic scattering, accurate differential cross sections are just now being determined experimentally, although integral and total cross sections for selected excitation processes have been available for many years for some species. Absolute DCS's for excitation of the $2s$ and $2p$ states of atomic hydrogen at low incident electron energies have recently been reported[2] and provide an excellent test[2,3] of numerous theories of electron-hydrogen scattering. Similarly, absolute DCS's over a range of incident electron energies and scattering angles have recently been reported[4,5] for the $n=2$ and 3 states of helium. As in the case of atomic hydrogen, these data now serve as reference data to which theories can be compared.[5] Although available DCS data for excitation of atomic hydrogen include only the $n=2$ states, the most complete theories appear to be working reasonably well for this particular target. However, for excitation of the $n=3$ states in helium, published theoretical results do not agree very well with experiment,[5,6] and this discrepancy has emphasized the need for improvements in the scattering theory for incident-electron energies above the ionization threshold.

Data have recently been reported[7-10] on the DCS's for excitation of complex atomic targets including Cu, Zn, Bi, and Pb, over a limited range of incident electron energies. In the case of Cu, the theory that has been applied[11] to treat elastic and inelastic scattering has been only partially successful and indicates a need for improved theories to treat atomic targets with complex electronic structure.

For inelastic electron-molecule collisions at low and intermediate incident electron energies, there is even less DCS information available than for electron-atom scattering. One of the first

measurements was carried out by Trajmar *et al.*, who reported[12] DCS's for excitation of the lowest sigma triplet state ($b\ ^3\Sigma_u^+$) in molecular hydrogen (at five incident electron energies) and compared the results to the predictions[12] of a first-order exchange (Ochkur-Rudge) theory. Trajmar *et al.*[13] reported DCS's for excitation of the $a\ ^1\Delta_g$ and $b\ ^1\Sigma_u^+$ states of O_2, at seven incident electron energies from 4 to 45 eV, and scattering angles from 10° to 90°. Linder and Schmidt[14] subsequently reported DCS's for the same two states from threshold to 7 eV and for scattering angles to 130°. Finally, Finn and Doering[15] have recently reported DCS's for excitation of the $a\ ^1\Pi_g$ state of N_2 over the angular range 0–90°, and for 14 incident electron energies from 13 to 100 eV.

It should be noted that except for the data of Linder and Schmidt[14] at low incident electron energies, previous measurements obtained DCS's only out to scattering angles of 90° so that information about large-angle scattering in inelastic scattering has not been available. All other studies of inelastic electron-molecule scattering have been confined to high incident electron energies, small scattering angles, or both. Lassettre and Skerbele[16] were pioneers in collecting and interpreting small momentum-transfer data in terms of the dipole spectrum of the target. Although these data reveal a great deal about optical and generalized oscillator strengths and the range of validity of the Born approximation, they contain relatively little information about optically forbidden transitions, and DCS's for optically allowed and forbidden transitions at low and intermediate electron energies.

Theoretical descriptions of inelastic electron-molecule scattering have been limited to those obtained with first-order theories because of the severe mathematical complexities associated with the application of improved theories to targets without spherical symmetry. Furthermore, the accuracy of these first-order[17] theories has been tested primarily against integral cross sections and has been found to be good in some cases and poor in others. However, what appears to be fairly good agreement between theory and experiment for integral cross sections[17] will be shown below to be poor agreement when comparing DCS's. This fact was illustrated by Julienne and Krauss[18] when they compared results from a first-order theory to experiment[13] for excitation of the $a\ ^1\Delta_g$ state of O_2. In this case, the theoretical DCS at 10 eV has an entirely different shape than the experimental DCS but, because of the $\sin\theta$ weighting of the DCS, the resulting *integral* cross sections differed by less than a factor of 2. The only other reported[12] comparison between theory and experiment for nonresonant inelastic scattering is for the excitation of the $b\ ^3\Sigma_u^+$ state of H_2. In this case, theoretical and experimental results are in fairly good agreement for incident electron energies of 35 eV and greater. The reason that DCS's predicted from a first-order theory should be reasonably good for transitions in H_2 but not for similar ones in O_2 is not clear without a reexamination of the details of those two cases. However, a detailed comparison between the measured DCS's for excitation of the states of N_2 and those predicted by first-order theories (in the last section of this paper) support the conclusions drawn by Julienne and Krauss.[18]

Except for off-resonance DCS's for excitation[13] of the lowest two excited states in O_2 and those for excitation[15] of the $a\ ^1\Pi_g$ state of N_2, there is no complete set of DCS's for any molecule that includes a large range of incident electron energies and/or many excited states of different symmetry.

This paper reports DCS's for excitation of the lowest six triplet and the lowest four singlet states of N_2 for seven incident electron energies from 10 to 50 eV. The following paper[19] presents integral cross sections for excitation of the same final states and compares them to both theory and experimental results obtained by different methods. The third paper in this series[20] reports DCS's and integral cross sections for excitation of nine singlet and triplet states in the range 12.5–14.2 eV above the molecular ground state.

II. EXPERIMENTAL

The measurements reported in this series of papers on the differential and integral cross sections were carried out over a period of four years using two electron-impact spectrometers of different design.

The *older instrument*[21] used hemispherical electrostatic energy selectors as the monochromator and analyzer in combination with simple-aperture lenses. For this instrument a typical energy resolution was 0.10 eV full width at half maximum (FWHM), and the angular range extended from −30° to +90°. The overall electron-detection efficiency was dependent, to some extent, on the kinetic energy of the electrons after scattering. For this reason, measurements using this spectrometer were limited to incident energies $E \geq 20$ eV, where the instrumental energy dependence was small relative to the statistical errors of the intensity measurements. The target gas was contained in a static gas chamber. The gas pressure and the incident electron beam current were monitored during the accumulation of an electron energy-loss spectrum to ensure identical experimental conditions for the recording of the whole spectrum. The incident electron energy scale was not cali-

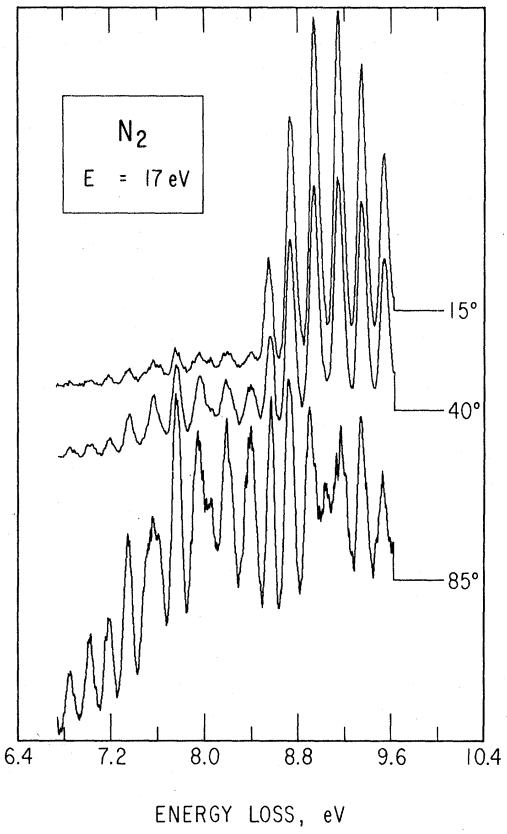

FIG. 1. Typical electron energy-loss spectra in N_2 obtained with the older instrument for 17-eV incident energy electrons and the three different scattering angles indicated in the figure.

brated and could have been in error by a few tenths of an eV due to contact potentials. At incident energies greater than 20 eV, this would have no significant effect on the results. A set of typical electron energy-loss spectra in N_2 obtained with this instrument is shown in Fig. 1.

The *newer instrument*, also described previously,[22,23] utilizes a crossed electron-beam molecular-beam geometry, and a much-improved electron-optics system using tube lenses and, as with the older instrument, hemispherical electrostatic analyzers. Typical energy resolution in the present work was 0.040 eV (FWHM) and the angular range covered was $-30° \leq \theta \leq 138°$ with an angular resolution[24] of about 2°. This newer instrument used a 7-element lens train as the analyzer optics, and the use of zoom and field lenses in this lens train ensured that the image properties (its size, location, and beam angle) at the entrance plane of the analyzer were insensitive to the kinetic energy of the electrons after scattering.[23] This feature allows one to compare reliably the intensity of an inelastic feature to the elastic-scattering intensity, or to the intensity of any other inelastic feature. Measurements of the electron energy-loss spectra in N_2 with this instrument were carried out at incident electron energies (E) of $10 \leq E \leq 50$ eV. The electron-energy scale was calibrated against the 19.35-eV He resonance (as measured in the elastic channel at 90° scattering angle) and the true-zero scattering angle was determined from the symmetry of inelastic scattering about the nominal-zero angle. The data-taking procedure was similar to that of the older instrument. Typical electron energy-loss spectra in N_2 obtained with the newer instrument are shown in Fig. 2.

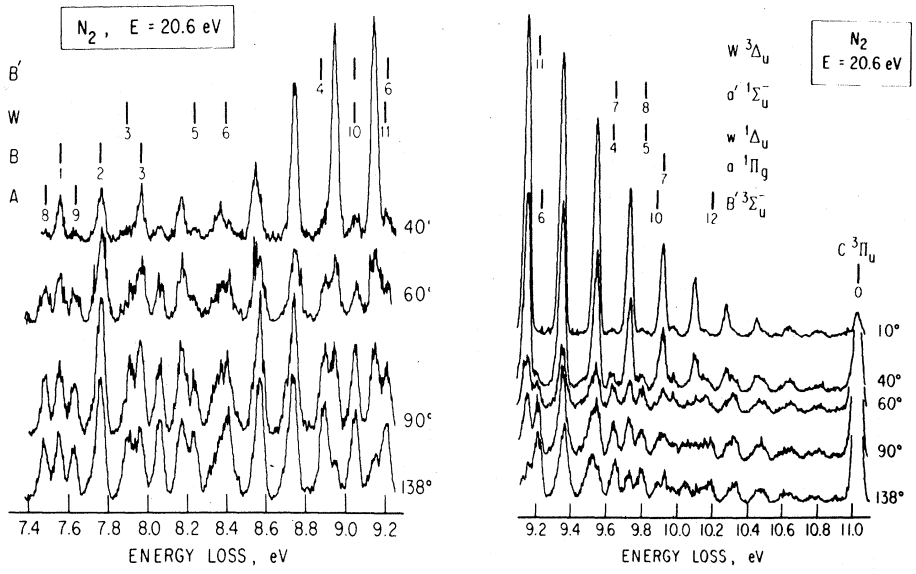

FIG. 2. Typical electron energy-loss spectra in N_2 obtained with the newer instrument at 20.6-eV incident energy and the scattering angles indicated in the figure. Comparison with the spectra in Fig. 1 shows the substantial improvement in energy resolution and background obtained with the newer instrument.

Data collected with both instruments consisted of the determination of the elastic-scattering intensity and the energy-loss spectra (scattered signal intensity vs energy loss) at a fixed scattering angle (θ) and E, over the energy-loss (W) range $7.1 \leq W \leq 11.1$ eV. Each spectrum was obtained as a superposition of repeated scans through the elastic peak ($W = 0$ eV) and the W range of interest utilizing pulse-counting and multichannel-scaling techniques.

From spectra such as those shown in Figs. 1 and 2, one obtains the intensity of each inelastic feature relative to any other inelastic feature and relative to the elastic peak. Many factors, such as "effective path-length" corrections, electron- and target-beam distributions, and long-term electron- and target-beam density fluctuations, cancel out in the ratio. The markedly different *shapes* of the elastic and inelastic DCS do, in principle, influence the effective path-length correction. However, this effect is estimated to be small (< 1%) and can be neglected. The relative intensities were obtained over the angular range $10° \leq \theta \leq 138°$, at incident energies of 10, 12.5, 15, 20, 30, and 50 eV. At incident electron energies and scattering angles for which the experimental measurements obtained with the two instruments overlapped, generally good agreement was found in the inelastic/elastic intensity ratios.

The 7.1–11.1-eV energy-loss region of N_2 consists of 8 electronic transitions with their concomitant overlapping vibrational bands. The handling of the large amount of data, and the unfolding of the many vibrational features from one another, was carried out by means of a spectral analysis technique discussed in the next section.

III. DATA ANALYSIS

A. Theory used in the data reduction

The analysis of electron energy-loss spectra in N_2 is particularly complicated because of overlapping of numerous vibrational levels from various electronic states for all energy losses greater than about 7 eV. The complexity of the energy-loss spectra is illustrated in Figs. 1 and 2 and the electronic-state potential-energy curves responsible for the overlapping features are shown in Fig. 3. The theoretical foundation upon which the data analysis technique is based is the following. Energy levels and Franck-Condon factors for excitation from the lowest vibrational level of the ground state to each vibrational level of each excited electronic state are assumed to be known, while the electronic portion of the intensities of the transitions are to be determined. Since the spacings of the rotational lines in N_2 are at least one order of magnitude smaller than the best instrumental energy resolution in this work, a rotationally averaged DCS can be used in the analysis, thereby leaving only the vibrational and electronic degrees of freedom to be treated. Furthermore, at these incident electron energies and energy losses, Doppler effects in the energy-loss

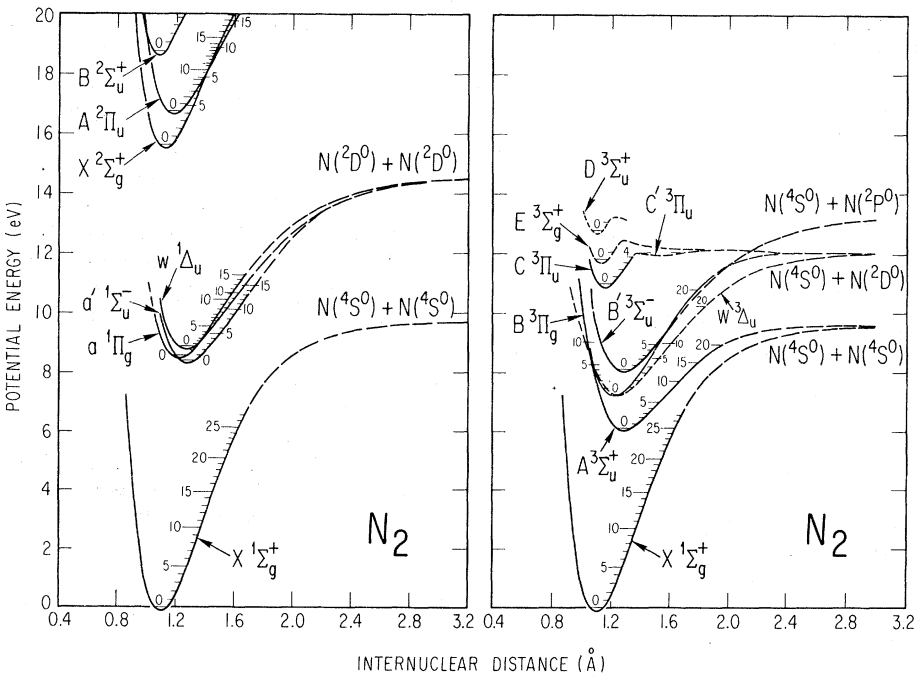

FIG. 3. Potential-energy curves for the lowest singlet (left panel) and triplet (right panel) states of N_2. The ground state is shown in both for reference purposes as are the N_2^+-ion states in the left panel. See text for description of the spectroscopic data used to obtained these curves.

spectra are small[25] relative to the instrumental resolution and can reasonably be neglected. With these assumptions, the analysis technique is developed along the lines given earlier,[13] with some modification as indicated below.

The rotationally averaged DCS for excitation of vibrational level v' of electronic state n' at incident energy E and scattering angle θ is denoted by $\sigma_{n'v'}(E,\theta)$. The scattered-electron current at energy loss W for an "ideal" measuring system of nearly perfect resolution is related to the total number of electronic transitions N, containing $M(n')$ vibrational bands, by

$$I_m(E,\theta,W') = \sum_{n'=0}^{N}\sum_{v'=0}^{M(n')} C(I_0,\rho,\Omega,F,\sigma)\sigma_{n'v'}(E,\theta) \times g_{n'v'}(W'-W_{n'v'}), \quad (1)$$

where $I_m(E,\theta,W')$ is the number of scattered electrons per second per steradian at impact energy E, scattering angle θ, and energy loss W' from a target gas of density ρ. The natural line shape of the $n''v''\rightarrow n'v'$ transition is characterized by $g_{n'v'}(W'-W_{n'v'})$. The quantity C is a complicated function that depends on the density distribution of the target gas (ρ), the incident electron beam current (I_0) distribution, the solid angle of the various scattering volume elements within the target beam at the detector (Ω), the detector efficiency (F), and, to some extent, on the variation of the DCS within the detector solid angle. This quantity (C) is kept constant at fixed E and θ and cancels out whenever intensity *ratios* from the same energy-loss spectrum are used, as long as the dependence of C on the DCS can be neglected. In the analysis of these data, this latter assumption has been made because model calculations indicate that no significant error is introduced by variations of the DCS's studied in this work.

In practice, energy-loss spectra are affected by resolution properties of the experimental apparatus such that the actual signal S is given by

$$S(E,\theta,W) = \int_{-\infty}^{\infty} I_m(E,\theta,W')F(W'-W)\,dW' + B(E,\theta,W,\rho,I_0), \quad (2)$$

where $F(W'-W)$ is a function which characterizes the effective resolution of the measuring device, and B denotes a background contribution to the measured signal. In the work reported here, the natural line shape is sufficiently narrower than the line shape produced by the analyzer that $g_{n'v'}$ can be approximated as a δ function in W' space. Equations (1) and (2) can then be combined and the integration over W' done immediately to give

$$S(E,\theta,W) = C\sum_{n'=0}^{N}\sum_{v'=0}^{M(n')}\sigma_{n'v'}(E,\theta)F(W_{n'v'}-W) + B(E,\theta,W,\rho,I_0). \quad (3)$$

Within the framework of the Born-Oppenheimer nuclear-electronic mass-separation approximation, the relative vibrational intensities are independent of incident energy and scattering angle so that $\sigma_{n'v'}$ can be written as

$$\sigma_{n'v'}(E,\theta) = \sigma_{n'}(E,\theta)\,q_{v'v''}, \quad (4)$$

where $q_{v'v''}$ is the Franck-Condon factor and $\sigma_{n'}$ now contains all the information concerning the angular dependence and absolute value of the DCS for a given electronic transition. Substituting Eq. (4) into Eq. (3), the scattered intensity becomes

$$S(E,\theta,W) = C\sum_{n'=0}^{N}\sigma_{n'}(E,\theta)\sum_{v'=0}^{M(n')}q_{v'v''}F(W_{n'v'}-W) + B(E,\theta,W,\rho,I_0). \quad (5)$$

One notes that because of the unknown factor C which appears in the above equations, the $\sigma_{n'}$ obtained for one incident energy cannot be *directly* compared to those measured at a different incident energy. The absolute calibration of these DCS's obtained at different incident energies will be discussed in Sec. III D.

During the time required to accumulate a spectrum, I_0 and ρ remain constant and, in all cases encountered, the background was well represented by the form

$$B(E,\theta,W) = \sum_{i=1}^{L} a_i(E,\theta)h_i(W), \quad (6)$$

where the h_i are known functions of the energy loss, and the coefficients $a_i(E,\theta)$ are to be determined by the analysis procedure.

The quantities $X_{n'}(E,\theta)\equiv C\sigma_{n'}(E,\theta)$ and $a_i(E,\theta)$ were determined for a given resolution in each spectrum from Eqs. (5) and (6) by requiring that the difference between the measured and calculated spectra be a minimum in a least-squares sense. That is, if $S_M(E,\theta,W)$ is the measured signal, then the quantity

$$\epsilon = \sum_{j=1}^{D}(S_M - S)^2 \quad (7)$$

is minimized, where D is the number of data points and S is as defined in Eq. (5). The canonical equations to be solved are obtained from (7) as

$$\frac{\partial\epsilon}{\partial X_{n'}} = 0, \quad n' = 1,\ldots,N$$
$$\frac{\partial\epsilon}{\partial a_i} = 0, \quad i = 1,\ldots,L \quad (8)$$

and represent a set of $N+L$ algebraic equations, the solution of which are the unknown coefficients $X_{n'}$ and a_i. With these coefficients, the scattered signal intensities at channels corresponding to the peak positions of the inelastic features are calculated. These calculated intensities are then divided by the elastic peak intensity appearing in the same spectrum to yield intensity ratios at each scattering angle and incident energy. Equations (8) are, in general, nonlinear because the instrumental resolution function $F(W_{n'v'}-W)$ is usually nearly Gaussian in character:

$$F(x)=(1/\Delta\sqrt{\pi})\exp(-x^2/\Delta^2), \tag{9}$$

where the quantity Δ denotes the functional full width at half maximum (FWHM). A convenient method by which Eqs. (8) can be solved that is, particularly well suited to computer implementation is to linearize these equations by assuming that the FWHM (Δ) is known. Different values of Δ are then chosen iteratively and the linearized Eqs. (8) repetitively solved until Eq. (7) is minimized.

In all the N_2 energy-loss spectra analyzed, the background (Eq. 6) was very well represented by a polynomial in the energy loss W:

$$h_i(W)=W^{i-1},\quad i=1,\ldots,4. \tag{10}$$

As shown by the lower curve in Fig. 1, the data taken on the older instrument contains a larger background contribution than those obtained on the newer instrument, particularly at the larger scattering angles. The computational technique employed, however, had no difficulty incorporating the steeply rising background in the early data.

B. Energy levels and Franck-Condon factors

The analysis techniques outlined above assume knowledge of the energy of each vibrational level for each excited state relative to $v'=0$ of the $X\,^1\Sigma_g^+$ state and the corresponding Franck-Condon factor. Data for the $A\,^3\Sigma_u^+$, $B\,^3\Pi_g$, $B'\,^3\Sigma_u^-$, $a'\,^1\Sigma_u^-$, $C\,^3\Pi_u$, and $a\,^1\Pi_g$ states were obtained by numerical integration[26] of the nuclear wave functions for the potential-energy curves of these states, as determined from the spectroscopic data of Benesch *et al.*[27] For the $W\,^3\Delta_u$ state, the recent results of Covey *et al.*[28] were used. The spectroscopic constants derived from the data of Tanaka *et al.*[29] were used to obtain the required quantities for the $w\,^1\Delta_u$ state. The results of Cartwright[17(a)] were used for the $E\,^3\Sigma_g^+$ state and the data of Ledbetter[30] for the $a''\,^1\Sigma_g^+$ state.

C. Example of the deconvolution

The computational technique described above[31] had been found to work remarkably well in extracting the relative contributions to one unresolved feature by two or three vibrational levels. This capability was particularly important in the analysis of the energy-loss data obtained with the older instrument because of the poorer resolution and stronger background contribution under certain circumstances. An example of the unfolding of data with a substantial background contribution from the older instrument is shown in Fig. 4 for a 2.8-eV region of the N_2 energy-loss spectrum. The lowest curve in this figure, the difference (data-fit) spectrum, provides a visual means for evaluating the quality of the unfolding procedure. The structure in the difference spectra is due to a combination of noise in the data, a slight error in the energy axis due to the digital nature of the data, deviations of the instrumental profile from the perfect Gaussian shape assumed in the analysis, and any breakdown in the Born-Oppenheimer approximation. Figure 5 illustrates the unfolding of a 6-eV region of the N_2 energy-loss spectrum obtained with the older instrument containing nine of the ten electronic states considered in this study. Although the nine electronic states in this energy-loss region contain a total of 148 vibrational levels, inspection of Fig. 5 reveals only about 30 peaks in the spectrum. This fact emphasizes the strongly overlapped nature of the N_2 energy-loss spectrum

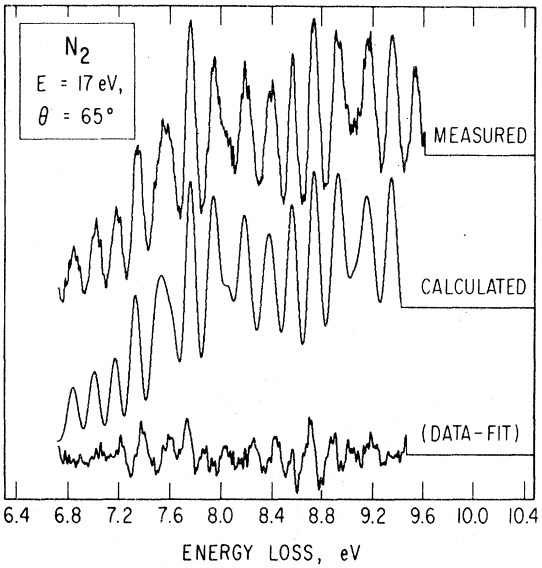

FIG. 4. Example of the spectral decomposition for data (17 eV, 65°) taken on the older instrument. The upper curve is the measured spectrum, the lower two are the calculated and difference spectra. A good portion of the structure present in this particular difference spectrum is believed to be due to a combination of asymmetric instrumental profile and a relatively large background signal.

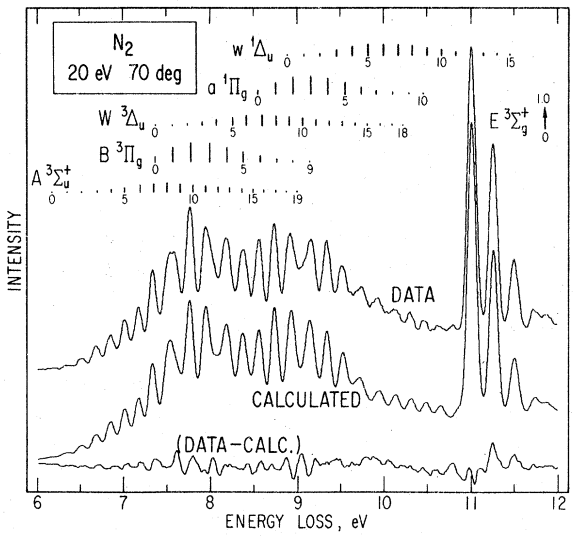

FIG. 5. A second example of the spectral decomposition of N_2 electron energy-loss data (20 eV, 70°) taken on the older instrument. This measured spectrum (upper curve) covers nearly the entire energy-loss region analyzed in this work and contains all the vibrational levels [Ref. 17(a)] of the nine lowest electronic states studied. Only the two vibrational levels associated with the a'' state do not appear in this spectral range. Vibrational levels of some of the electronic states are indicated in the figure by the vertical lines whose heights are proportional to the appropriate Franck-Condon factor for excitation from the ground state. As is the case in Fig. 4, the structure in the difference spectrum is believed due to an asymmetric line shape and a strong background.

and the indispensability of a computer technique to accurately determine the DCS for each electronic state. Comparison of the calculated spectrum with the data, and examination of the difference spectrum, leads to the conclusion that the analysis technique generally does very well in fitting the spectrum. None of the N_2 data analyzed showed any indication that the Born-Oppenheimer approximation was breaking down for electron-impact excitation of N_2.

The results shown in Figs. 4 and 5 were obtained in 1972 but the DCS values obtained from the unfolding procedure were so surprising that it was not certain that they could be believed. Because the DCS values obtained were much larger than expected, it was thought that perhaps the numerical techniques used to deconvolute the spectra were introducing spurious values for certain electronic states (such as the $W\,^3\Delta_u$, $w\,^1\Delta_u$, $B'\,^3\Sigma_u^-$, and $a'\,^1\Sigma_u^-$ states) for which no individual vibrational levels could be seen in the data (from the older instrument). Construction of the newer machine described above was completed at about that time, and it was decided to take additional N_2 spectra at higher resolution in order to check the DCS results and to extend the angular coverage from 90 to 138 deg. Examples of the spectra taken with the newer instrument are shown in Fig. 2 and the deconvolution of selected spectra at the same energy is shown in Fig. 6. Comparisons of Figs. 4 and 6 emphasizes the increased resolution and much lower background of the data obtained with the newer instrument and the increased transparency of the data in terms of identifying vibrational levels

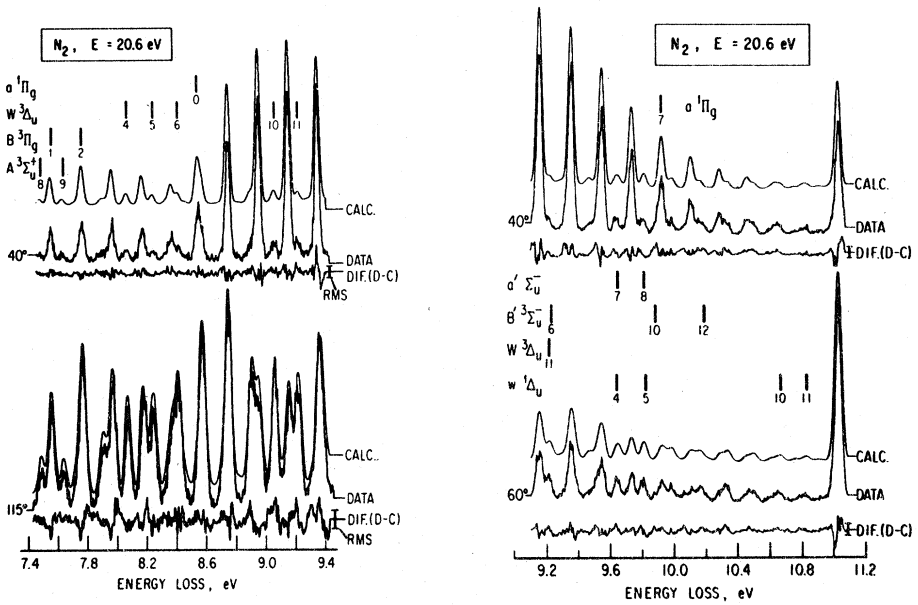

FIG. 6. Examples of the spectral decomposition of N_2 electron energy-loss spectra (20.6 eV; 40°, 60°, 115°) taken on the newer instrument. Certain vibrational levels of some of the electronic states that can be readily identified in the spectra are shown in the figure by the vertical lines. The higher resolution in these data allowed the first identification of peaks in the spectra associated with the B', a', W, and w states.

from the various electronic states. The data shown in Fig. 6 represented the first identification[22] of the W, w, B', and a' states in electron energy-loss spectra and, in addition, verified that the deconvolution of the spectra from the older machine was, in fact, correct.

In more detail, the computer analysis procedure involved choosing one particular inelastic feature containing little or no contribution from more than one vibrational level [usually $C\ ^3\Pi_u(v'=0)$ or $A\ ^3\Sigma_u^+(v'=6)$] as a reference peak and accurately determining its location in each energy-loss spectrum by minimizing the rms for small variations of its channel location in the digitized spectrum. The reference peak determined in this fashion was always within one or two channels of that calculated from spectroscopic data and the location of the elastic peak. The elastic-peak location was taken as the zero energy-loss channel, even though there is a slight angle- and energy-dependent deviation of the elastic peak from the zero energy-loss value as a result of momentum transfer to the target. The largest value of this shift (at $E=50$ eV and $\theta=138°$) is 0.005 eV and can therefore be neglected for the present data. The above procedure determined the energy-loss axis in each spectrum to within an accuracy of one-half the energy-loss step size used to collect the data (either 0.002 or 0.004 eV, depending on the spectrum). The nonlinear parameter, the instrumental FWHM, was then varied and the "best" deconvolution of a spectrum was assumed to have been found when the rms was minimized. The computer technique included the search procedures described above which were repeated until the process converged. Contributions from vibrational levels of each electronic state that appeared in each spectrum were then summed and, if necessary, renormalized (if the spectrum did not cover all vibrational levels) for a given state to provide the total contribution from each electronic state to that particular energy-loss spectrum.

The above procedure resulted in the relative contribution of each electronic state to an energy-loss spectrum at a particular incident electron energy and scattering angle. From the assumptions used in the theory of the analysis techniques, Eqs. (4) and (5), these relative contributions are just the relative DCS values for excitation of the electronic states at that incident energy and scattering angle. These relative DCS's were made absolute in the manner described in Sec. III D.

D. Normalization of the DCS's

By determining the inelastic/elastic ratio for one particular inelastic feature for each energy-loss spectrum analyzed, and using known *absolute elastic* DCS's, all the relative inelastic DCS's were placed on an absolute scale. Since each energy-loss spectrum corresponds to one particular incident energy and scattering angle, absolute elastic DCS's were needed for the same incident energy and scattering angle as used for the inelastic data. The required absolute elastic DCS's were either taken directly (for 10, 15, 20, and 50 eV) from the recent measurements of Srivastava *et al.*[1] or interpolated (for 12.5 and 17 eV) from the elastic DCS's measured above and below the specific energy of interest.

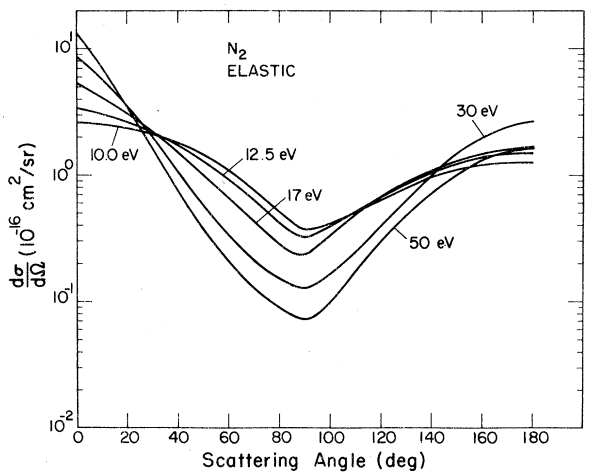

FIG. 7. Differential cross sections (DCS's) for elastic scattering of electrons by N_2 at five incident electron energies. Values for incident energies of 12.5 and 17 eV were interpolated from the data at higher and lower energies reported in Ref. 1.

The elastic DCS's used in this work to convert the relative inelastic DCS's into absolute DCS's are shown in Fig. 7 and tabulated in Table I. The elastic DCS's are believed to be accurate to about 15% and are presented here, along with the inelastic/elastic calibration, so that improved inelastic DCS's can be obtained from the present data should better elastic DCS's become available in the future. Peak heights for $C\ ^3\Pi_u(v'=0)$ and/or $A\ ^3\Sigma_u^+(v'=6)$, which contain little or no contribution from other transitions, were determined from all the spectra and converted to an intensity for exciting the *entire* electronic state by dividing by the appropriate Franck-Condon factor. The quantities determined at each scattering angle and incident energy were divided by the appropriate elastic-scattering intensity to give the inelastic/elastic ratios shown in Figs. 8 and 9. At 10-eV incident electron energy the C state is not excited (threshold 11.032 eV), and at 12.5 eV the intensity of the C state in the inelastic spectra could not be accurately determined. $A\ ^3\Sigma_u^+$ elastic ratios were

TABLE I. Differential cross sections (cm^2/sr), *elastic*.[1] The notation $N-n$ means $N\times10^{-n}$.

Angle (deg)	Energy (eV) 10	12.5	15.0	17.0	20.0	30.0	50.0
0	0.259 – 15	0.343 – 15	0.411 – 15	0.530 – 15	0.644 – 15	0.863 – 15	0.119 – 14
10	0.251 – 15	0.316 – 15	0.366 – 15	0.422 – 15	0.473 – 15	0.582 – 15	0.640 – 15
20	0.233 – 15	0.271 – 15	0.296 – 15	0.313 – 15	0.327 – 15	0.361 – 15	0.311 – 15
30	0.210 – 15	0.224 – 15	0.226 – 15	0.225 – 15	0.222 – 15	0.201 – 15	0.146 – 15
40	0.178 – 15	0.174 – 15	0.160 – 15	0.150 – 15	0.139 – 15	0.104 – 15	0.658 – 16
50	0.141 – 15	0.130 – 15	0.113 – 15	0.102 – 15	0.895 – 16	0.602 – 16	0.329 – 16
60	0.108 – 15	0.965 – 16	0.802 – 16	0.691 – 16	0.573 – 16	0.361 – 16	0.192 – 16
70	0.752 – 16	0.647 – 16	0.506 – 16	0.432 – 16	0.352 – 16	0.211 – 16	0.114 – 16
80	0.505 – 16	0.433 – 16	0.341 – 16	0.291 – 16	0.236 – 16	0.151 – 16	0.914 – 17
90	0.363 – 16	0.322 – 16	0.266 – 16	0.235 – 16	0.201 – 16	0.125 – 16	0.676 – 17
100	0.450 – 15	0.433 – 16	0.396 – 16	0.356 – 16	0.312 – 16	0.164 – 16	0.877 – 17
110	0.501 – 16	0.508 – 16	0.491 – 16	0.475 – 16	0.453 – 16	0.236 – 16	0.155 – 16
120	0.622 – 16	0.650 – 16	0.647 – 16	0.644 – 16	0.634 – 16	0.381 – 16	0.265 – 16
130	0.772 – 16	0.832 – 16	0.852 – 16	0.853 – 16	0.845 – 16	0.622 – 16	0.430 – 16
140	0.942 – 16	0.105 – 15	0.110 – 15	0.109 – 15	0.106 – 15	0.983 – 16	0.649 – 16
150	0.108 – 15	0.124 – 15	0.133 – 15	0.129 – 15	0.123 – 15	0.144 – 15	0.905 – 16
160	0.118 – 15	0.139 – 15	0.152 – 15	0.144 – 15	0.135 – 15	0.194 – 15	0.118 – 15
170	0.122 – 15	0.148 – 15	0.167 – 15	0.157 – 15	0.144 – 15	0.233 – 15	0.139 – 15
180	0.123 – 15	0.152 – 15	0.173 – 15	0.162 – 15	0.150 – 15	0.161 – 15	0.148 – 15

therefore used with the absolute elastic DCS's to normalize the relative DCS's at these energies. At the other energies, the $C\ ^3\Pi_u$ elastic ratios were used with the absolute elastic DCS's to normalize the relative inelastic DCS's. The peak in the inelastic/elastic *ratio* that appears in Figs. 8 and 9 at all energies considered in this work near 90° scattering angle is due primarily to a minimum in the elastic DCS's near 90° as shown in Fig. 7. Data obtained with both the old and the new instruments were used to construct Figs. 8 and 9,

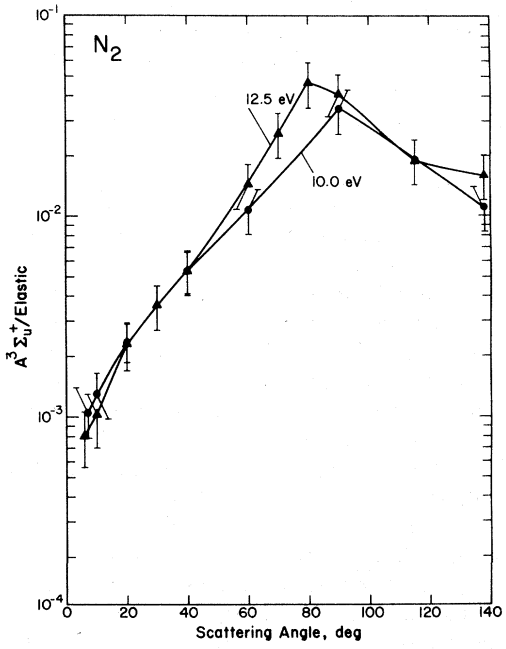

FIG. 8. Ratio of the DCS for excitation of the *A* state to that for elastic scattering as a function of the scattering angle for two incident electron energies. The error bars shown represent the combined error in determining the inelastic and elastic peak intensities in the energy-loss spectra. The peak in this ratio is due primarily to the minima in the elastic DCS near 90° scattering angle.

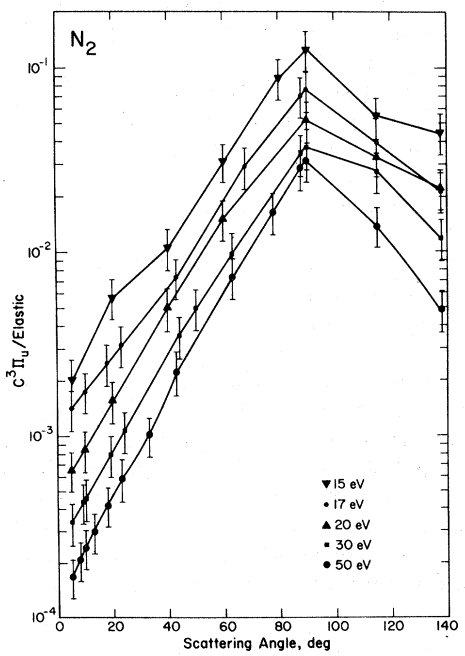

FIG. 9. Ratio of the DCS for excitation of the *C* state to that for elastic scattering for five incident electron energies. See Fig. 8 for additional details.

and there was generally excellent agreement in the inelastic ratios obtained from the two instruments wherever they overlapped. Straight lines have been drawn to connect the data points since only the values of the ratio at the data points shown were used to construct the DCS. The error bars shown, generally about 25%, represent a conservative estimate of the error in the inelastic/elastic ratio and includes consideration of both the accuracy and the precision of the measurements.

E. Error analysis

The computational technique used to analyze the data (Sec. III A) was designed to include a determination of the uncertainty (expressed as a standard deviation) in the value derived for each electronic state used in the deconvolution of the energy-loss spectrum. Because of the least-squares basis of this computational technique, the uncertainty associated with each electronic state is a measure of how sensitive the deconvolution of the entire energy-loss spectrum is to a variation in the strength of the DCS for that particular electronic state. In more qualitative terms, the uncertainty in the contribution from a particular electronic state to a given energy-loss spectrum will generally be much larger for a state for which no vibrational levels are visible (in the spectrum) than for a state whose vibrational levels dominate the spectrum. Since *errors* in both the inelastic/elastic ratio and the elastic DCS are almost the same for all scattering angles, the deconvolution error discussed above is of primary importance in accurately determining the *shapes* of each inelastic DCS. In the following section, where the inelastic DCS's are discussed, the error bars shown in the figures are only the deconvolution errors and do not include contributions from the errors in the inelastic/elastic ratio or in the magnitude of the elastic DCS.

IV. RESULTS

The number of electron energy-loss spectra required to cover the angular region sufficiently to yield an accurate DCS at each incident electron energy results in an amount of data which is far too large to be included here in its entirety. A few representative examples of the electron energy-loss spectra from both the old and new instruments have been included here, but space limitations do not allow the other spectra to be shown. For similar reasons, figures showing the derived DCS values and error bars at the measured angles are also given here only for 10-, 12.5-, 20-, and 50-eV incident electron energies, rather than for all seven incident energies studied. As many of these figures as possible have been included in order to illustrate how the shapes of the DCS's have been obtained from the data points. These figures also serve to illustrate how the DCS's for excitation of certain of the electronic states are more accurately determined than for others as a result of some inelastic features being relatively weak in all the energy-loss spectra. The N_2 electron energy-loss and DCS data not presented here are being collected together and will appear as a monograph[32] in the near future.

A. DCS's at fixed incident electron energy

Figures 10–13 show the DCS data points and uncertainties as obtained from the electron energy-loss spectra (at 10, 12.5, 20, and 50 eV) at various scattering angles and illustrate how smooth curves have been drawn through the data points to obtain the DCS's. In all these figures, an error

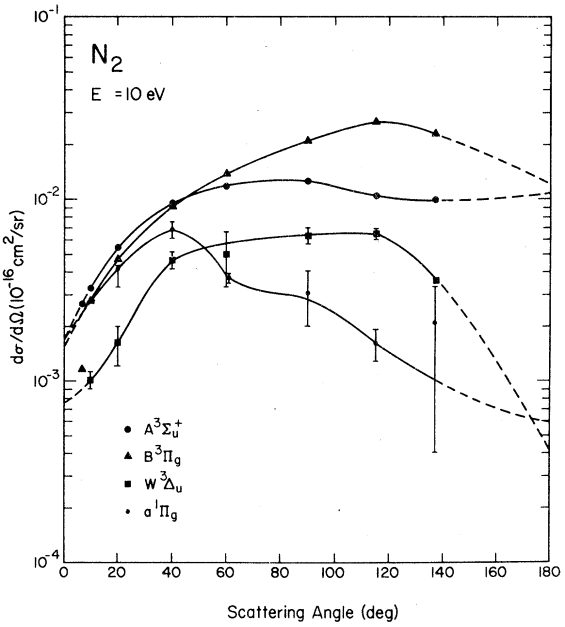

FIG. 10. DCS's for excitation of the A, B, W, and a states of N_2 at 10-eV incident electron energy illustrating how the DCS curves were drawn through the data. Error bars are shown only if larger than the data-point symbols. As discussed in the text, the larger the error bar, the more weakly present is that particular state in the data at that specific scattering angle. Smooth curves have been drawn through the data points wherever possible, but in some cases the "most reasonable" curve does not pass directly through those data points with large error bars. The dashed portion of each curve denotes the regions of extrapolation to scattering angles of 0 and 180°. These four electronic states are the only ones that could be obtained from the energy-loss data at 10-eV incident energy.

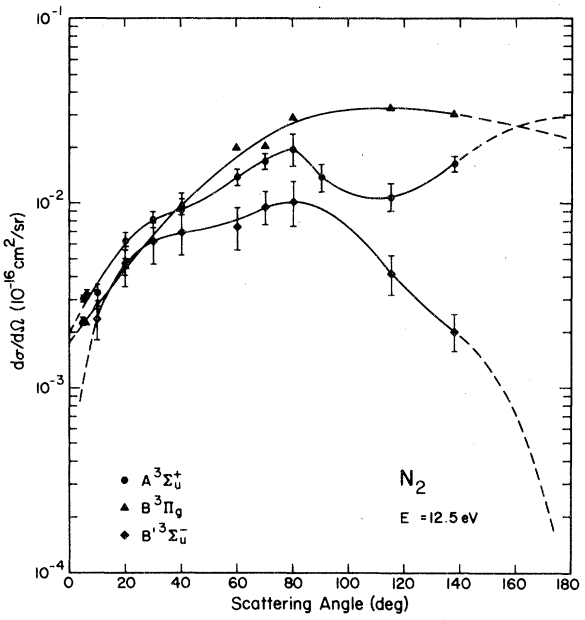

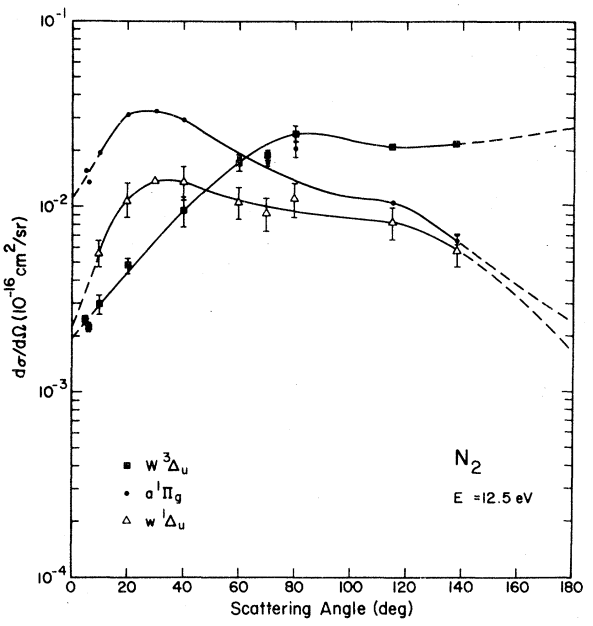

FIG. 11. Same as Fig. 10, but for an incident electron energy of 12.5 eV and for the A, B, W, a, B', and w states. See Fig. 10 for additional details.

bar is shown only when larger than the symbol used to denote the data point. In some cases, the smooth DCS curve has been drawn somewhat arbitrarily because of large error bars on certain data points. As a result of this procedure, the uncertainty in the shape of the DCS for certain electronic states at certain incident energies may be somewhat greater than the average uncertainty in the other DCS's. An example of this is the DCS for the $a\,^1\Pi_g$ state at 10 eV, shown in Fig. 10, which is considerably more uncertain at the large scattering angles than the DCS's for the other states determined at 10 eV because of the large error bar associated with the 138° data point.

The DCS's shown in Figs. 10–13 were extrapolated to scattering angles of 0 and 180° by drawing smooth curves through the data points. Particular attention was paid to DCS's at small scattering angles because of their relationship to the generalized oscillator strength. The DCS's for the various electronic states, as a function of the incident electron energy, approach 0° scattering angle in such a variety of ways that it was found essential to have data at 5° in order to estimate DCS's at 0°. Electron energy-loss spectra from both instruments were used to construct the DCS's and, in the few cases where the results from the two sets of data disagreed, a preference toward the data from the new instrument was employed in drawing the DCS's.

B. DCS's as a function of the incident electron energy

1. States with triplet character

Figures 14–17 show the DCS's for excitation of the $A\,^3\Sigma_u^+$, $B\,^3\Pi_g$, $W\,^3\Delta_u$, and $C\,^3\Pi_u$ states at the seven different incident electron energies studied in this work. These four states are characterized by DCS's that generally increase as the scattering angle increases, which distinguishes them from the DCS's for the other states studied. For each of these four states there are one or more energies for which the DCS does not strictly increase monotonically but, generally speaking, the DCS's for these states have a small forward scattering component and a large backscattering component. The most notable exception to this behavior is the DCS for excitation of the $W\,^3\Delta_u$ at 10 eV which appears to have a weak backscattering component. The cause for this different shape is not clear but is perhaps due to a combination of the Δ symmetry of the final state and the fact that the incident electron energy is close to the excitation threshold.

The DCS's for excitation of the $A\,^3\Sigma_u^+$ state all demonstrate a peculiarity for which there is presently no clear explanation. That is, as seen in Fig. 14, the DCS's all show a dip at a scattering angle near 115°. Additional energy-loss data were taken around 115° at a few selected incident energies to be sure the appearance of the dip was not instrumental in origin. All the data indicate that the dip is a genuine property of the $A\,^3\Sigma_u^+$ state and does not appear in any of the other DCS's studied in this work (except possibly the $C\,^3\Pi_u$ state at 15 eV). An explanation for this dip that

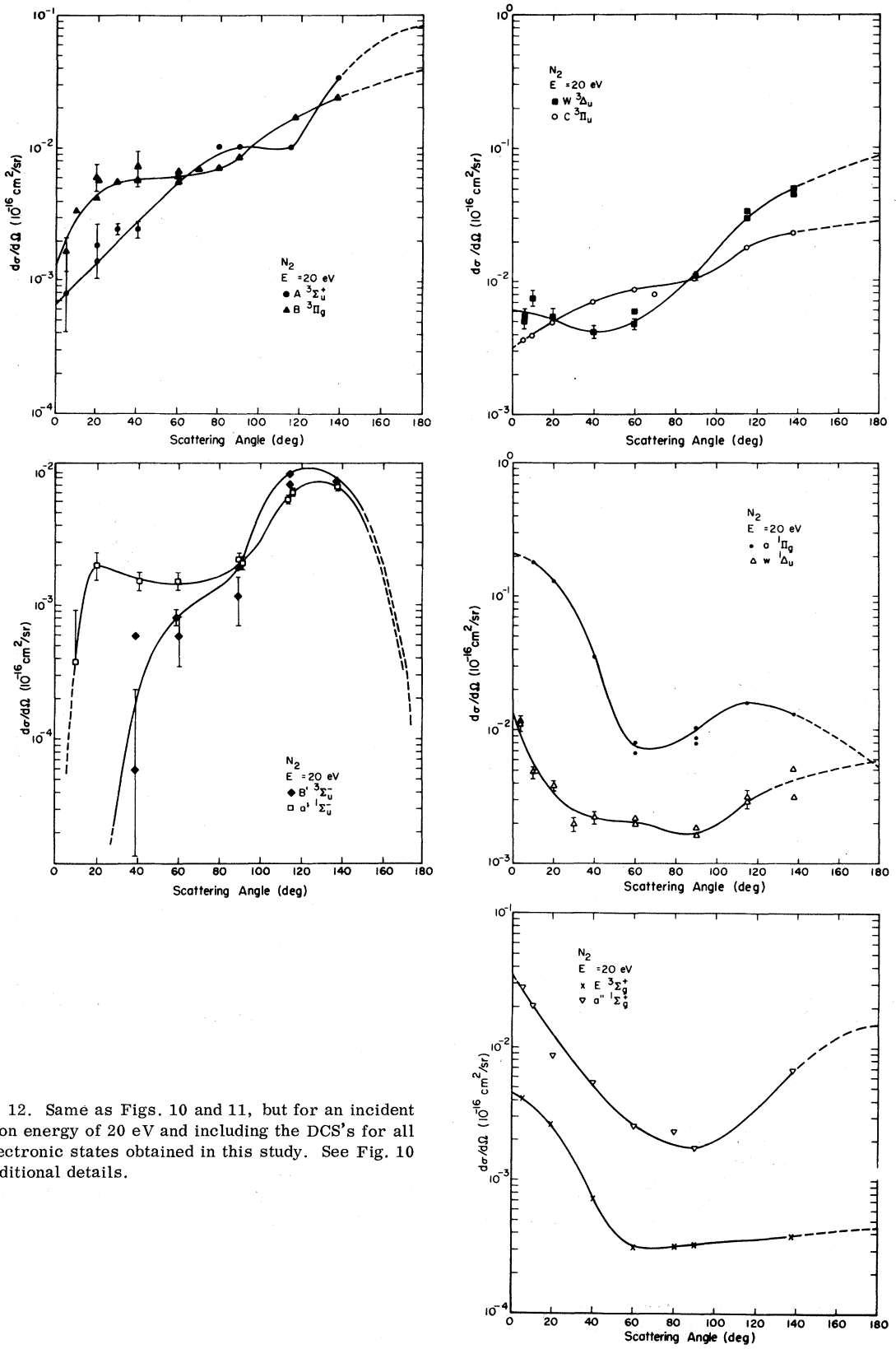

FIG. 12. Same as Figs. 10 and 11, but for an incident electron energy of 20 eV and including the DCS's for all ten electronic states obtained in this study. See Fig. 10 for additional details.

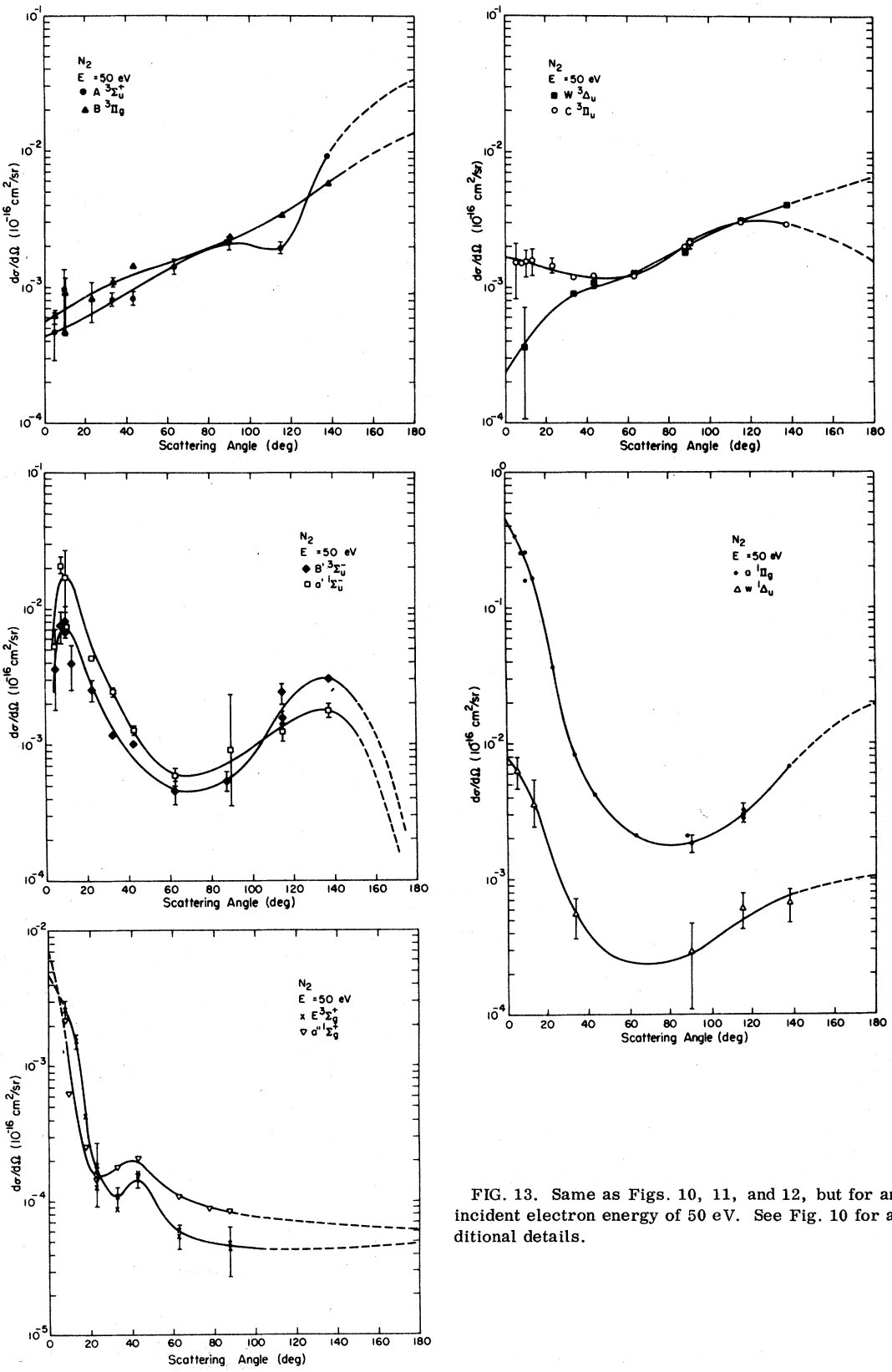

FIG. 13. Same as Figs. 10, 11, and 12, but for an incident electron energy of 50 eV. See Fig. 10 for additional details.

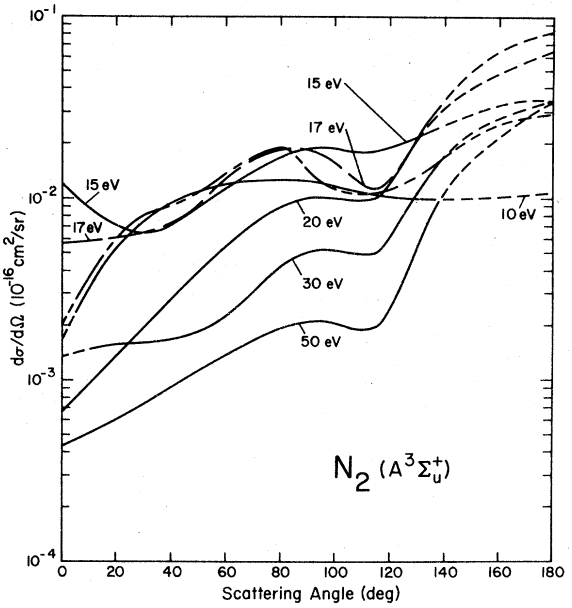

FIG. 14. DCS's for excitation of the A state for seven incident electron energies. The curves shown in this figure were obtained by drawing smooth curves through data points as illustrated in Figs. 10–13. The data points and error bars have been omitted for purposes of clarity.

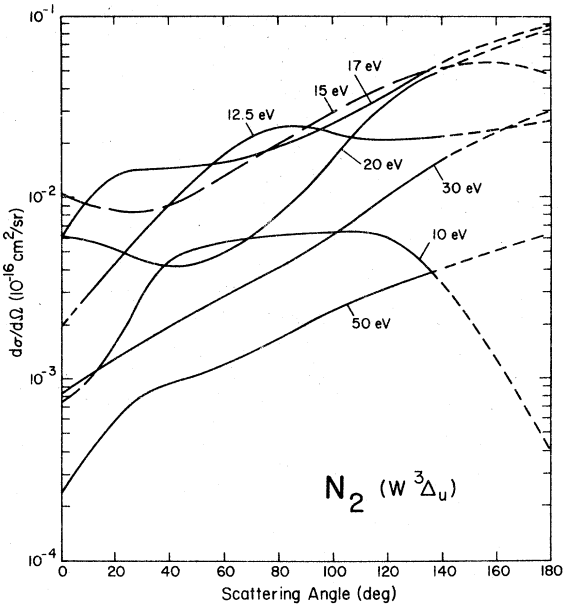

FIG. 16. DCS's for excitation of the W state for seven incident electron energies. See Fig. 14 for additional details.

comes to mind is that it is related to a broad resonance process involving the A state. Recent measurements[33] have identified a core-excited shape resonance, with the A state as the parent, which has an effect on A-state excitation cross sections. The aspect of the present results that is difficult to explain is that the dip shown in Fig. 14 is present for incident electron energies from 12.5 to at least 50 eV, while the resonance observed by Mazeau *et al.*[33] extends only over the 9–11-eV region. For this reason, this observed narrow resonance

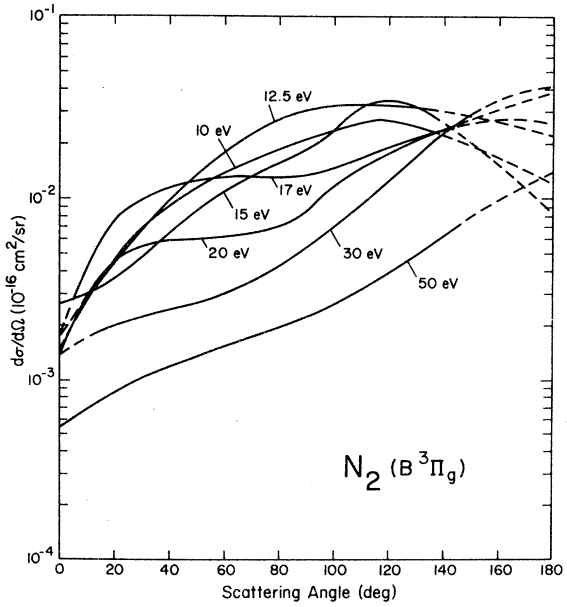

FIG. 15. DCS's for excitation of the B state for seven incident electron energies. See Fig. 14 for additional details.

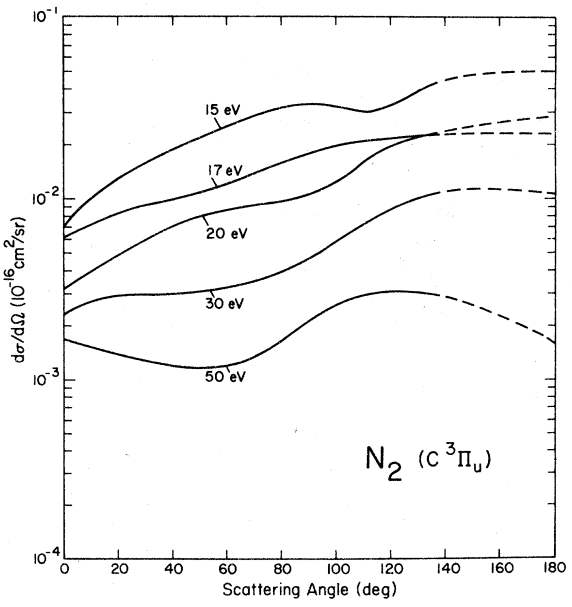

FIG. 17. DCS's for excitation of the C state for five incident electron energies. See Fig. 14 for additional details.

TABLE II. Differential cross sections (cm^2/sr), $A\,^3\Sigma_u^+$. $N-n$ means $N\times10^{-n}$.

Angle (deg)	Energy (eV) 10	12.5	15.0	17.0	20.0	30.0	50.0
0	0.168 – 18	0.203 – 18	0.122 – 17	0.569 – 18	0.653 – 19	0.132 – 18	0.430 – 19
10	0.330 – 18	0.373 – 18	0.883 – 18	0.588 – 18	0.957 – 19	0.147 – 18	0.512 – 19
20	0.545 – 18	0.621 – 18	0.698 – 18	0.617 – 18	0.140 – 18	0.154 – 18	0.612 – 19
30	0.754 – 18	0.813 – 18	0.649 – 18	0.664 – 18	0.197 – 18	0.159 – 18	0.740 – 19
40	0.954 – 18	0.915 – 18	0.712 – 18	0.759 – 18	0.280 – 18	0.167 – 18	0.896 – 19
50	0.108 – 17	0.110 – 17	0.897 – 18	0.949 – 18	0.397 – 18	0.182 – 18	0.111 – 18
60	0.117 – 17	0.138 – 17	0.114 – 17	0.131 – 17	0.548 – 18	0.225 – 18	0.137 – 18
70	0.124 – 17	0.167 – 17	0.141 – 17	0.165 – 17	0.733 – 18	0.301 – 18	0.165 – 18
80	0.127 – 17	0.192 – 17	0.168 – 17	0.186 – 17	0.898 – 18	0.409 – 18	0.192 – 18
90	0.124 – 17	0.137 – 17	0.191 – 17	0.185 – 17	0.102 – 17	0.506 – 18	0.216 – 18
100	0.117 – 17	0.113 – 17	0.189 – 17	0.157 – 17	0.102 – 17	0.518 – 18	0.208 – 18
110	0.107 – 17	0.108 – 17	0.182 – 17	0.120 – 17	0.992 – 18	0.498 – 18	0.194 – 18
120	0.102 – 17	0.113 – 17	0.189 – 17	0.132 – 17	0.125 – 17	0.602 – 18	0.244 – 18
130	0.995 – 18	0.135 – 17	0.215 – 17	0.213 – 17	0.224 – 17	0.108 – 17	0.525 – 18
140	0.987 – 18	0.172 – 17	0.253 – 17	0.323 – 17	0.350 – 17	0.169 – 17	0.103 – 17
150	0.987 – 18	0.218 – 17	0.290 – 17	0.408 – 17	0.490 – 17	0.226 – 17	0.158 – 17
160	0.102 – 17	0.260 – 17	0.322 – 17	0.493 – 17	0.642 – 17	0.277 – 17	0.215 – 17
170	0.105 – 17	0.284 – 17	0.342 – 17	0.569 – 17	0.759 – 17	0.320 – 17	0.260 – 17
180	0.109 – 17	0.294 – 17	0.344 – 17	0.645 – 17	0.855 – 17	0.345 – 17	0.283 – 17

is most likely not responsible for all the characteristics of the dip observed around 115° scattering angle.

The DCS's for excitation of the $B\,^3\Pi_g$, $W\,^3\Delta_u$, and $C\,^3\Pi_u$ possess no particularly striking characteristics that persist at all incident energies other than the trend toward backscattering discussed above.

The DCS for excitation of the W state at 10 eV appears to have an anomalously small backscattering component, and there appears to be a dip in the DCS for excitation of the C state near 115° at 15-eV incident energy, but these effects do not appear to be present at other incident electron energies. Another interesting property that the DCS's for the

TABLE III. Differential cross section (cm^2/sr), $B\,^3\Pi_g$. $N-n$ means $N\times10^{-n}$.

Angle (deg)	Energy (eV) 10	12.5	15.0	17.0	20.0	30.0	50.0
0	0.152 – 18	0.169 – 18	0.268 – 18	0.180 – 18	0.128 – 18	0.137 – 18	0.567 – 19
10	0.273 – 18	0.271 – 18	0.296 – 18	0.436 – 18	0.286 – 18	0.169 – 18	0.695 – 19
20	0.465 – 18	0.452 – 18	0.350 – 18	0.759 – 18	0.438 – 18	0.198 – 18	0.859 – 18
30	0.682 – 18	0.666 – 18	0.467 – 18	0.996 – 18	0.543 – 18	0.221 – 18	0.112 – 18
40	0.930 – 18	0.949 – 18	0.655 – 18	0.116 – 17	0.584 – 18	0.243 – 18	0.122 – 18
50	0.114 – 17	0.133 – 17	0.854 – 18	0.125 – 17	0.600 – 18	0.261 – 18	0.137 – 18
60	0.137 – 17	0.177 – 17	0.111 – 17	0.133 – 17	0.609 – 18	0.293 – 18	0.153 – 18
70	0.162 – 17	0.226 – 17	0.132 – 17	0.134 – 17	0.642 – 18	0.345 – 18	0.174 – 18
80	0.185 – 17	0.271 – 17	0.157 – 17	0.133 – 17	0.703 – 18	0.417 – 18	0.196 – 18
90	0.210 – 17	0.299 – 17	0.185 – 17	0.136 – 17	0.840 – 18	0.530 – 18	0.224 – 18
100	0.234 – 17	0.317 – 17	0.236 – 17	0.148 – 17	0.114 – 17	0.690 – 18	0.261 – 18
110	0.257 – 17	0.324 – 17	0.313 – 17	0.169 – 17	0.145 – 17	0.915 – 18	0.314 – 18
120	0.263 – 17	0.323 – 17	0.347 – 17	0.195 – 17	0.177 – 17	0.123 – 17	0.388 – 18
130	0.245 – 17	0.314 – 17	0.319 – 17	0.220 – 17	0.209 – 17	0.170 – 17	0.489 – 18
140	0.221 – 17	0.298 – 17	0.262 – 17	0.245 – 17	0.244 – 17	0.231 – 17	0.621 – 18
150	0.193 – 17	0.280 – 17	0.205 – 17	0.262 – 17	0.274 – 17	0.285 – 17	0.795 – 18
160	0.167 – 17	0.260 – 17	0.157 – 17	0.275 – 17	0.307 – 17	0.339 – 17	0.987 – 18
170	0.143 – 17	0.239 – 17	0.114 – 17	0.273 – 17	0.344 – 17	0.385 – 17	0.118 – 17
180	0.120 – 17	0.218 – 17	0.854 – 18	0.261 – 17	0.385 – 17	0.409 – 17	0.136 – 17

TABLE IV. Differential cross sections (cm^2/sr), $W\,^3\Delta_u$. $N-n$ means $N\times10^{-n}$.

Angle (deg)	Energy (eV) 10	12.5	15.0	17.0	20.0	30.0	50.0
0	0.754 – 19	0.192 – 18	0.107 – 17	0.607 – 18	0.607 – 18	0.803 – 19	0.238 – 19
10	0.102 – 18	0.294 – 18	0.934 – 18	0.977 – 18	0.578 – 18	0.102 – 18	0.402 – 19
20	0.160 – 18	0.441 – 18	0.854 – 18	0.131 – 17	0.518 – 18	0.128 – 18	0.621 – 19
30	0.297 – 18	0.655 – 18	0.840 – 18	0.143 – 17	0.453 – 18	0.159 – 18	0.841 – 19
40	0.465 – 18	0.938 – 18	0.925 – 18	0.147 – 17	0.420 – 18	0.195 – 18	0.996 – 19
50	0.529 – 18	0.129 – 17	0.111 – 17	0.152 – 17	0.438 – 18	0.233 – 18	0.110 – 18
60	0.569 – 18	0.169 – 17	0.134 – 17	0.159 – 17	0.502 – 18	0.282 – 18	0.124 – 18
70	0.602 – 18	0.215 – 17	0.164 – 17	0.173 – 17	0.619 – 18	0.341 – 18	0.146 – 18
80	0.618 – 18	0.243 – 17	0.202 – 17	0.194 – 17	0.817 – 18	0.417 – 18	0.176 – 18
90	0.634 – 18	0.241 – 17	0.245 – 17	0.228 – 17	0.112 – 17	0.506 – 18	0.215 – 18
100	0.646 – 18	0.224 – 17	0.299 – 17	0.266 – 17	0.168 – 17	0.634 – 18	0.254 – 18
110	0.642 – 18	0.211 – 17	0.362 – 17	0.313 – 17	0.245 – 17	0.803 – 18	0.293 – 18
120	0.602 – 18	0.207 – 17	0.424 – 17	0.384 – 17	0.333 – 17	0.102 – 17	0.334 – 18
130	0.465 – 18	0.210 – 17	0.478 – 17	0.470 – 17	0.420 – 17	0.130 – 17	0.379 – 18
140	0.329 – 18	0.215 – 17	0.518 – 17	0.569 – 17	0.508 – 17	0.162 – 17	0.430 – 18
150	0.213 – 18	0.225 – 17	0.547 – 17	0.664 – 17	0.595 – 17	0.199 – 17	0.480 – 18
160	0.128 – 18	0.237 – 17	0.552 – 17	0.759 – 17	0.677 – 17	0.236 – 17	0.539 – 18
170	0.730 – 19	0.249 – 17	0.529 – 17	0.844 – 17	0.770 – 17	0.271 – 17	0.603 – 18
180	0.401 – 19	0.263 – 17	0.484 – 17	0.902 – 17	0.863 – 17	0.301 – 17	0.676 – 18

A, B, and W states share is a generally weak forward scattering at the lower incident energies that increases as the incident energy increases. Although this trend appears to be followed fairly well for these states, it is not a dominant effect and appears to have some exceptions as noted in Fig. 16 for the W state at 15 and 50 eV. Tabulated DCS's for the A, B, W, and C states are given in Tables II–V respectively.

2. *States with Σ^- character*

The only rigorous selection rule for inelastic electron-molecule scattering presently known is

TABLE V. Differential cross sections (cm^2/sr), $C\,^3\Pi_u$. $N-n$ means $N\times10^{-n}$.

Angle (deg)	Energy (eV) 15.0	17.0	20.0	30.0	50.0
0	0.712 – 18	0.626 – 18	0.315 – 18	0.225 – 18	0.165 – 18
10	0.994 – 18	0.740 – 18	0.397 – 18	0.281 – 18	0.152 – 18
20	0.128 – 17	0.844 – 18	0.490 – 18	0.285 – 18	0.137 – 18
30	0.158 – 17	0.949 – 18	0.595 – 18	0.289 – 18	0.126 – 18
40	0.188 – 17	0.102 – 17	0.700 – 18	0.293 – 18	0.118 – 18
50	0.219 – 17	0.112 – 17	0.794 – 18	0.305 – 18	0.114 – 18
60	0.248 – 17	0.123 – 17	0.863 – 18	0.321 – 18	0.119 – 18
70	0.285 – 17	0.140 – 17	0.910 – 18	0.349 – 18	0.137 – 18
80	0.316 – 17	0.161 – 17	0.957 – 18	0.393 – 18	0.166 – 18
90	0.333 – 17	0.180 – 17	0.105 – 17	0.466 – 18	0.215 – 18
100	0.322 – 17	0.199 – 17	0.121 – 17	0.586 – 18	0.259 – 18
110	0.305 – 17	0.210 – 17	0.155 – 17	0.731 – 18	0.291 – 18
120	0.330 – 17	0.219 – 17	0.190 – 17	0.867 – 18	0.303 – 18
130	0.396 – 17	0.226 – 17	0.212 – 17	0.987 – 18	0.302 – 18
140	0.453 – 17	0.228 – 17	0.230 – 17	0.108 – 17	0.286 – 18
150	0.481 – 17	0.231 – 17	0.245 – 17	0.112 – 17	0.257 – 18
160	0.495 – 17	0.235 – 17	0.257 – 17	0.112 – 17	0.224 – 18
170	0.507 – 17	0.235 – 17	0.267 – 17	0.108 – 17	0.190 – 18
180	0.507 – 17	0.234 – 17	0.277 – 17	0.104 – 17	0.155 – 18

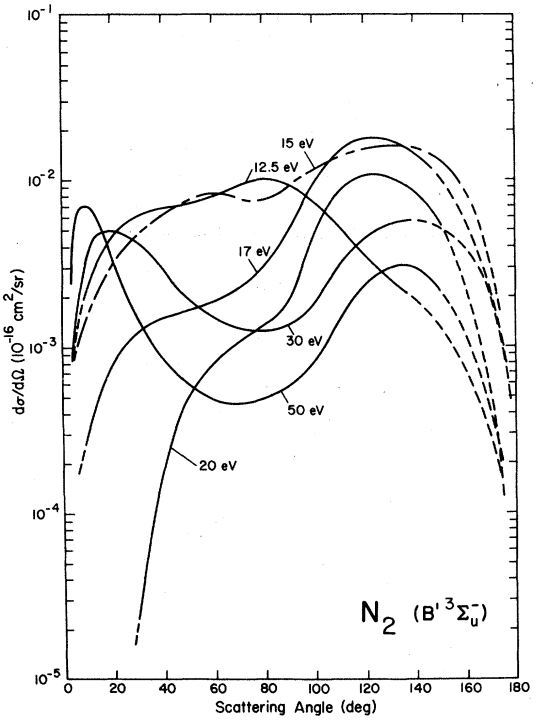

FIG. 18. DCS's for excitation of the B' state for six incident electron energies. The extrapolated portions of the curves that may be uncertain are shown by the short-dashed lines. See Fig. 14 for additional details.

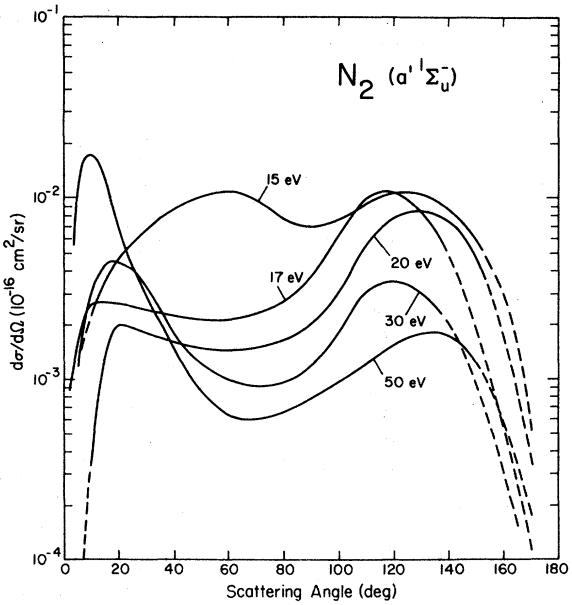

FIG. 19. DCS's for excitation of the a' state for five incident electron energies. See Figs. 14 and 18 for additional details.

that the DCS for a $\Sigma^+ \leftrightarrow \Sigma^-$ transition is identically zero at 0° and 180° scattering angles. This selection rule was discovered during the analysis[13] of electron energy-loss data in O_2 (for the $\Sigma_g^- \rightarrow \Sigma_g^+$ transition) and was later proven theoretically[34] to apply to all linear molecules. The only case for which this selection rule has been observed previously is the ($^3\Sigma_g^- \rightarrow {}^1\Sigma_g^+$) excitation in O_2, and in that case, the DCS's did not extend beyond 90°.

Figures 18 and 19 show the DCS's for excitation of the $B'\,{}^3\Sigma_g^-$ and $a'\,{}^1\Sigma_u^-$ states of N_2 for a number of different incident electron energies. Both sets of DCS's demonstrate a dramatic fall-off at small

TABLE VI. Differential cross sections (cm^2/sr), $B'\,{}^3\Sigma_u^-$. $N-n$ means $N\times10^{-n}$.

Angle (deg)	Energy (eV) 12.5	15.0	17.0	20.0	30.0	50.0
0	0.113 – 19	0.285 – 20	0.949 – 21	0.117 – 20	0.803 – 21	0.914 – 21
10	0.237 – 18	0.157 – 18	0.361 – 19	0.117 – 20	0.377 – 18	0.731 – 18
20	0.463 – 18	0.313 – 18	0.797 – 19	0.117 – 20	0.498 – 18	0.347 – 18
30	0.621 – 18	0.484 – 18	0.125 – 18	0.233 – 20	0.425 – 18	0.256 – 18
40	0.689 – 18	0.626 – 18	0.152 – 18	0.187 – 19	0.289 – 18	0.914 – 19
50	0.734 – 18	0.755 – 18	0.166 – 18	0.490 – 19	0.193 – 18	0.612 – 19
60	0.813 – 18	0.840 – 18	0.190 – 18	0.817 – 19	0.152 – 18	0.494 – 19
70	0.949 – 18	0.789 – 18	0.232 – 18	0.107 – 18	0.132 – 18	0.466 – 19
80	0.103 – 17	0.774 – 18	0.318 – 18	0.135 – 18	0.127 – 18	0.503 – 19
90	0.926 – 18	0.940 – 18	0.503 – 18	0.198 – 18	0.137 – 18	0.594 – 19
100	0.734 – 18	0.115 – 17	0.977 – 18	0.496 – 18	0.193 – 18	0.841 – 19
110	0.520 – 18	0.137 – 17	0.148 – 17	0.852 – 18	0.317 – 18	0.137 – 18
120	0.350 – 18	0.151 – 17	0.175 – 17	0.106 – 17	0.522 – 18	0.228 – 18
130	0.260 – 18	0.159 – 17	0.171 – 17	0.104 – 17	0.558 – 18	0.297 – 18
140	0.192 – 18	0.157 – 17	0.144 – 17	0.852 – 18	0.578 – 18	0.302 – 18
150	0.135 – 18	0.134 – 17	0.103 – 17	0.560 – 18	0.522 – 18	0.219 – 18
160	0.791 – 19	0.854 – 18	0.569 – 18	0.233 – 18	0.385 – 18	0.123 – 18
170	0.339 – 19	0.342 – 18	0.218 – 18	0.537 – 19	0.201 – 18	0.457 – 19
180	0.113 – 19	0.285 – 20	0.949 – 21	0.117 – 20	0.803 – 21	0.914 – 21

TABLE VII. Differential cross sections (cm^2/sr), $a'\,^1\Sigma_u^-$. $N-n$ means $N \times 10^{-n}$.

Angle (deg)	Energy (eV) 15.0	17.0	20.0	30.0	50.0
0	0.285 – 20	0.949 – 21	0.117 – 20	0.803 – 21	0.914 – 21
10	0.228 – 18	0.199 – 18	0.373 – 19	0.281 – 18	0.160 – 17
20	0.455 – 18	0.266 – 18	0.152 – 18	0.434 – 18	0.731 – 18
30	0.669 – 18	0.247 – 18	0.177 – 18	0.325 – 18	0.297 – 18
40	0.854 – 18	0.223 – 18	0.154 – 18	0.181 – 18	0.149 – 18
50	0.103 – 17	0.214 – 18	0.146 – 18	0.120 – 18	0.868 – 19
60	0.111 – 17	0.218 – 18	0.144 – 18	0.987 – 19	0.640 – 19
70	0.982 – 18	0.235 – 18	0.149 – 18	0.907 – 19	0.603 – 19
80	0.769 – 18	0.273 – 18	0.166 – 18	0.947 – 19	0.649 – 19
90	0.683 – 18	0.365 – 18	0.203 – 18	0.119 – 18	0.758 – 19
100	0.755 – 18	0.626 – 18	0.303 – 18	0.177 – 18	0.950 – 19
110	0.920 – 18	0.977 – 18	0.560 – 18	0.289 – 18	0.121 – 18
120	0.107 – 17	0.106 – 17	0.782 – 18	0.337 – 18	0.154 – 18
130	0.104 – 17	0.854 – 18	0.852 – 18	0.301 – 18	0.178 – 18
140	0.868 – 18	0.503 – 18	0.735 – 18	0.201 – 18	0.176 – 18
150	0.598 – 18	0.190 – 18	0.467 – 18	0.939 – 19	0.128 – 18
160	0.285 – 18	0.531 – 19	0.175 – 18	0.321 – 19	0.612 – 19
170	0.569 – 19	0.123 – 19	0.350 – 19	0.803 – 20	0.192 – 19
180	0.285 – 20	0.949 – 21	0.117 – 20	0.803 – 21	0.914 – 21

scattering angles, and these present results are the first to indicate that the DCS's also fall off at 180°. Inspection of these two figures also reveals another interesting characteristic of the DCS's. Namely, as the incident electron energy increases, the DCS develops a well pronounced double-peaked shape and the forward-scattering peak increases while the backscattering peak decreases. The DCS's for these two states are remarkably similar, the only apparent differences being that those for the a' state have a somewhat stronger forward peak (compared to that for the B' state at the same energy), while those for the B' state are slightly more isotropic at the lower energies with a slightly larger backscattering peak. It is interesting to note that the cross section for excitation of either of these states is identically zero in the Born, Ochkur-Rudge, or equivalent approximation.[17(a)] It is also noted that, due to the double-peaked nature of the DCS's, an angular momentum analysis of the $\Sigma^+ \rightarrow \Sigma^-$ excitation process will likely be complicated. Tabulated DCS's for the B' and a' states are given in Tables VI and VII, respectively.

3. *States with singlet character*

Figures 20–22 show the DCS's for excitation of the $a\,^1\Pi_g$ and $w\,^1\Delta_u$ states for a number of different incident electron energies. For incident electron energies greater than 12.5 eV for the a state, and 30 eV for the w state, these DCS's are characterized by relatively strong forward peaking, particularly for the a state. Although the uncertainties in the DCS's for the w state are relatively large, it is still fairly certain that these DCS's are not *strongly* forward peaked except for energies greater than 30 eV. As will be discussed in Sec. IV B 1,

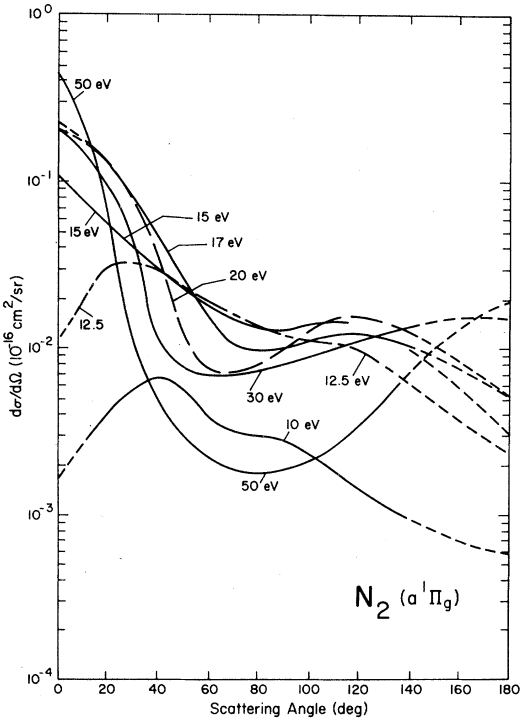

FIG. 20. DCS's for excitation of the a state for seven incident electron energies. See Figs. 14 and 18 for additional details.

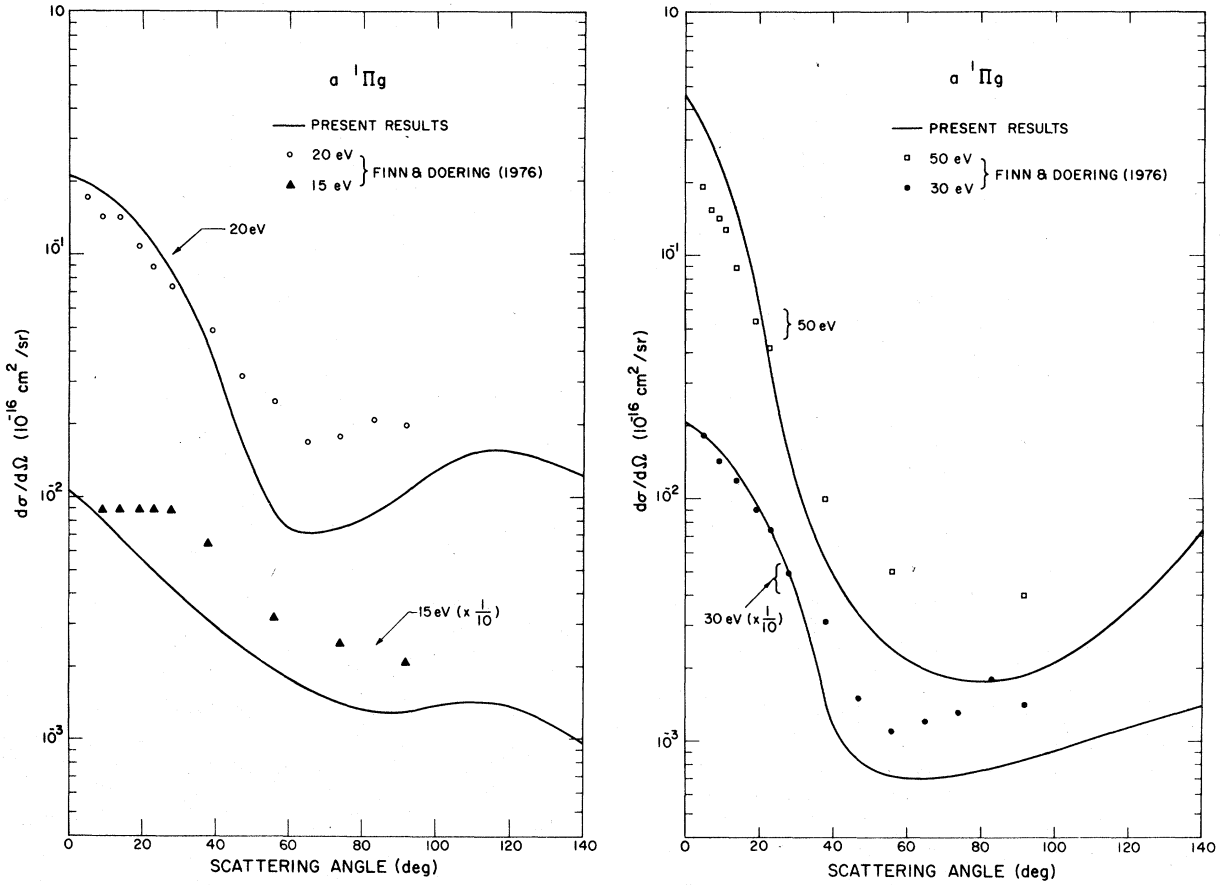

FIG. 21. Comparison of the DCS's for excitation of the a state obtained in this study with those obtained by Finn and Doering for four different incident electron energies. See text for further discussion.

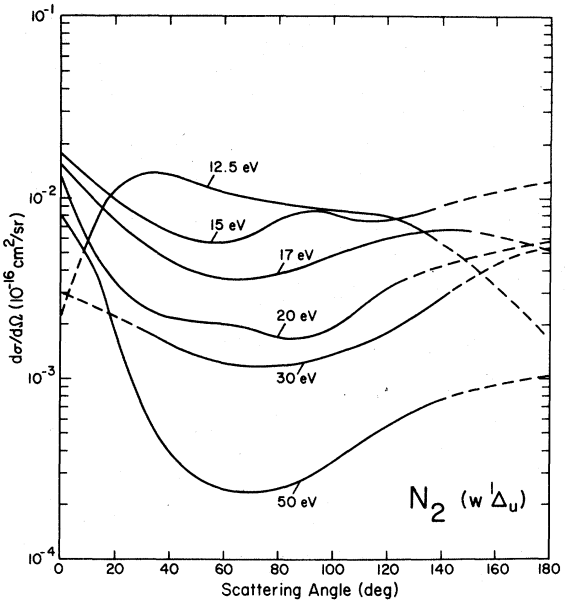

FIG. 22. DCS's for excitation of the w state for six incident electron energies. See Figs. 14 and 18 for additional details.

a qualitative model for excitation of singlet states would predict strong forward peaking in the DCS's.

The present DCS results for excitation of the $a\,^1\Pi_g$ state are compared in Fig. 21 with the results of Finn and Doering,[15] who obtained DCS's by visual inspection of electron energy-loss data in N_2. The angular measurements of Finn and Doering only extended to 92° scattering angle and, for lack of other information, they assumed a constant value for the DCS's from 92 to 180°. For scattering angles less than about 40°, the results of Finn and Doering are in good agreement with the present measurements except at 15 eV. For angles greater than 40°, Fig. 21 shows that the values of the DCS's deduced by Finn and Doering are generally greater than the present results. This is most likely due to the fact that their data analysis scheme did not account for the numerous vibrational levels from other electronic states (e.g., a', B', W, w) that exist in the same energy-loss region as the $a\,^1\Pi_g$ state. Since these states have appreciable excitation cross sections at intermediate scattering angles (see Figs. 16, 18, 19, and

TABLE VIII. Differential cross sections (cm^2/sr), $a\,^1\Pi_g$. $N-n$ means $N\times10^{-n}$.

Angle (deg)	Energy (eV) 10	12.5	15.0	17.0	20.0	30.0	50.0
0	0.168 – 18	0.113 – 17	0.108 – 16	0.238 – 16	0.210 – 16	0.209 – 16	0.457 – 16
10	0.277 – 17	0.192 – 17	0.797 – 17	0.185 – 16	0.177 – 16	0.153 – 16	0.228 – 16
20	0.417 – 18	0.311 – 17	0.555 – 17	0.130 – 16	0.129 – 16	0.939 – 17	0.621 – 17
30	0.557 – 18	0.325 – 17	0.399 – 17	0.826 – 17	0.770 – 17	0.401 – 17	0.113 – 17
40	0.682 – 18	0.289 – 17	0.293 – 17	0.503 – 17	0.350 – 17	0.120 – 17	0.494 – 18
50	0.569 – 18	0.234 – 17	0.228 – 17	0.285 – 17	0.131 – 17	0.779 – 18	0.298 – 18
60	0.369 – 18	0.191 – 17	0.182 – 17	0.161 – 17	0.747 – 18	0.698 – 18	0.223 – 18
70	0.325 – 18	0.159 – 17	0.154 – 17	0.113 – 17	0.729 – 18	0.706 – 18	0.186 – 18
80	0.301 – 18	0.137 – 17	0.134 – 17	0.101 – 17	0.805 – 18	0.747 – 18	0.176 – 18
90	0.285 – 18	0.120 – 17	0.131 – 17	0.104 – 17	0.992 – 18	0.819 – 18	0.183 – 18
100	0.237 – 18	0.112 – 17	0.140 – 17	0.117 – 17	0.128 – 17	0.899 – 18	0.210 – 18
110	0.185 – 18	0.107 – 17	0.145 – 17	0.126 – 17	0.152 – 17	0.101 – 17	0.260 – 18
120	0.140 – 18	0.983 – 18	0.140 – 17	0.127 – 17	0.155 – 17	0.114 – 17	0.343 – 18
130	0.104 – 18	0.802 – 18	0.122 – 17	0.120 – 17	0.143 – 17	0.127 – 17	0.494 – 18
140	0.726 – 19	0.621 – 18	0.996 – 18	0.107 – 17	0.124 – 17	0.140 – 17	0.731 – 18
150	0.553 – 19	0.474 – 18	0.783 – 18	0.854 – 18	0.105 – 17	0.149 – 17	0.102 – 17
160	0.401 – 19	0.373 – 18	0.598 – 18	0.797 – 18	0.852 – 18	0.154 – 17	0.135 – 17
170	0.281 – 19	0.294 – 18	0.427 – 18	0.664 – 18	0.665 – 18	0.157 – 17	0.167 – 17
180	0.201 – 19	0.237 – 18	0.313 – 18	0.531 – 18	0.513 – 18	0.154 – 17	0.192 – 17

22), their neglect in the data analysis will lead to an overestimation of the DCS for excitation of the $a\,^1\Pi_g$ state. The present results also show that, particularly at the higher incident electron energies, the DCS's are not constant for scattering angles greater than 90°, as assumed by Finn and Doering.[15] The DCS's for excitation of the a and w states are tabulated in Tables VIII and IX, respectively.

4. States with Rydberg character

The DCS's for excitation of the $E\,^3\Sigma_g^+$ and $a''\,^1\Sigma_g^+$ ($3s\sigma_g$) Rydberg states, shown in Figs. 23 and 24, contain a peculiar hump near 40° scattering angle, for incident electron energies at 30 eV and above. Furthermore, for incident electron energies of 17 eV and greater, the DCS's for excitation of the E state appear to be strongly forward peaked and

TABLE IX. Differential cross sections (cm^2/sr), $w\,^1\Delta_u$. $N-n$ means $N\times10^{-n}$.

Angle (deg)	Energy (eV) 12.5	15.0	17.0	20.0	30.0	50.0
0	0.203 – 18	0.177 – 17	0.166 – 17	0.128 – 17	0.297 – 18	0.804 – 18
10	0.542 – 18	0.131 – 17	0.114 – 17	0.572 – 18	0.259 – 18	0.457 – 18
20	0.106 – 17	0.982 – 18	0.778 – 18	0.338 – 18	0.223 – 18	0.178 – 18
30	0.135 – 17	0.783 – 18	0.579 – 18	0.253 – 18	0.185 – 18	0.695 – 19
40	0.133 – 17	0.655 – 18	0.465 – 18	0.222 – 18	0.156 – 18	0.402 – 19
50	0.116 – 17	0.581 – 18	0.408 – 18	0.210 – 18	0.133 – 18	0.283 – 19
60	0.105 – 17	0.567 – 18	0.370 – 18	0.204 – 18	0.122 – 18	0.238 – 19
70	0.983 – 18	0.626 – 18	0.351 – 18	0.189 – 18	0.119 – 18	0.238 – 19
80	0.926 – 18	0.755 – 18	0.389 – 18	0.170 – 18	0.120 – 18	0.256 – 19
90	0.881 – 18	0.854 – 18	0.446 – 18	0.170 – 18	0.127 – 18	0.292 – 19
100	0.847 – 18	0.811 – 18	0.503 – 18	0.198 – 18	0.138 – 18	0.356 – 19
110	0.825 – 18	0.746 – 18	0.560 – 18	0.251 – 18	0.154 – 18	0.448 – 19
120	0.779 – 18	0.766 – 18	0.617 – 18	0.323 – 18	0.183 – 18	0.567 – 19
130	0.666 – 18	0.814 – 18	0.664 – 18	0.385 – 18	0.225 – 18	0.676 – 19
140	0.553 – 18	0.911 – 18	0.683 – 18	0.436 – 18	0.287 – 18	0.786 – 19
150	0.429 – 18	0.996 – 18	0.674 – 18	0.478 – 18	0.369 – 18	0.877 – 19
160	0.316 – 18	0.110 – 17	0.636 – 18	0.518 – 18	0.441 – 18	0.941 – 19
170	0.237 – 18	0.117 – 17	0.579 – 18	0.554 – 18	0.502 – 18	0.101 – 18
180	0.169 – 18	0.125 – 17	0.522 – 18	0.584 – 18	0.538 – 18	0.106 – 18

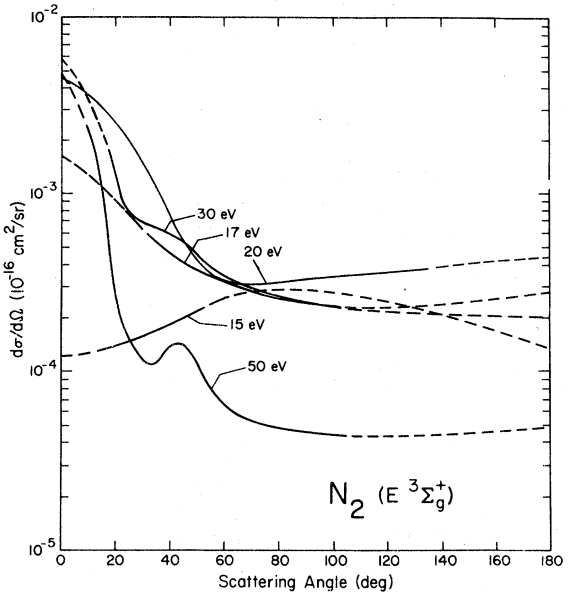

FIG. 23. DCS's for excitation of the E state for five incident electron energies. See Figs. 14 and 18 for additional details.

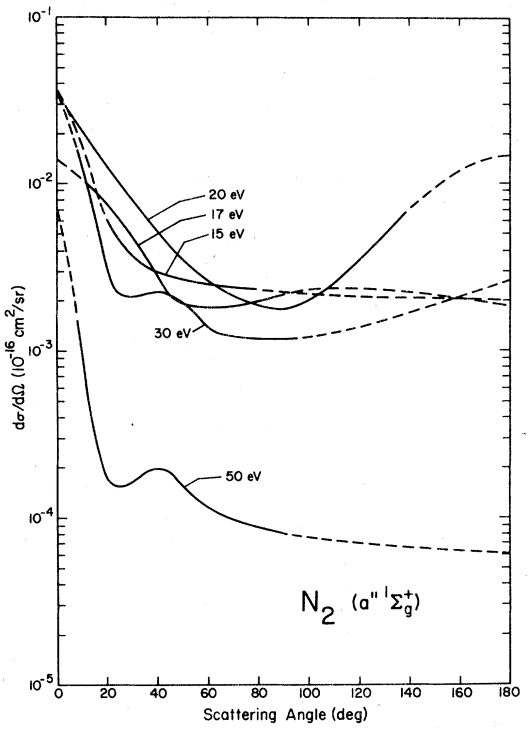

FIG. 24. DCS's for excitation of the a'' state for five incident electron energies. See Figs. 14 and 18 for additional details.

very similar in shape to those for the a'' state. Although the data for the E state at incident energies of 15 and 17 eV were not as good as for the higher energies, they seem to show the DCS's to be small at small scattering angles for incident energies less than 17 eV, and then become forward peaked at the higher energies. The generalized oscillator strength for the $X\ ^1\Sigma_g^+ \rightarrow a''\ ^1\Sigma_g^+$ transition has been reported[16] but nothing peculiar was noted at that time, perhaps because sufficiently large values of the momentum transfer were not studied in those experiments. The similarity of

TABLE X. Differential cross sections (cm^2/sr), $E\ ^3\Sigma_g^+$. $N-n$ means $N \times 10^{-n}$.

Angle (deg)	Energy (eV) 15.0	17.0	20.0	30.0	50.0
0	0.122 – 19	0.313 – 19	0.455 – 18	0.594 – 18	0.457 – 18
10	0.128 – 19	0.361 – 19	0.303 – 18	0.337 – 18	0.228 – 18
20	0.140 – 19	0.380 – 19	0.163 – 18	0.132 – 18	0.274 – 19
30	0.157 – 19	0.389 – 19	0.665 – 19	0.682 – 19	0.114 – 19
40	0.182 – 19	0.380 – 19	0.292 – 19	0.594 – 19	0.139 – 19
50	0.219 – 19	0.351 – 19	0.245 – 19	0.450 – 19	0.111 – 19
60	0.256 – 19	0.323 – 19	0.245 – 19	0.345 – 19	0.658 – 20
70	0.276 – 19	0.285 – 19	0.257 – 19	0.289 – 19	0.539 – 20
80	0.285 – 19	0.266 – 19	0.280 – 19	0.257 – 19	0.484 – 20
90	0.285 – 19	0.247 – 19	0.315 – 19	0.241 – 19	0.457 – 20
100	0.276 – 19	0.237 – 19	0.362 – 19	0.225 – 19	0.448 – 20
110	0.262 – 19	0.228 – 19	0.432 – 19	0.225 – 19	0.439 – 20
120	0.245 – 19	0.218 – 19	0.513 – 19	0.225 – 19	0.439 – 20
130	0.225 – 19	0.209 – 19	0.607 – 19	0.225 – 19	0.430 – 20
140	0.205 – 19	0.199 – 19	0.735 – 19	0.233 – 19	0.430 – 20
150	0.185 – 19	0.190 – 19	0.863 – 19	0.233 – 19	0.420 – 20
160	0.168 – 19	0.180 – 19	0.980 – 19	0.241 – 19	0.420 – 20
170	0.151 – 19	0.171 – 19	0.108 – 18	0.241 – 19	0.411 – 20
180	0.134 – 19	0.161 – 19	0.117 – 18	0.249 – 19	0.411 – 20

TABLE XI. Differential cross sections (cm^2/sr), $a''\,^1\Sigma_g^+$. $N-n$ means $N \times 10^{-n}$.

Angle (deg)	Energy (eV) 15.0	17.0	20.0	30.0	50.0
0	0.370 – 17	0.142 – 17	0.338 – 17	0.369 – 17	0.731 – 17
10	0.171 – 17	0.108 – 17	0.204 – 17	0.136 – 17	0.110 – 17
20	0.626 – 18	0.769 – 18	0.126 – 17	0.329 – 18	0.174 – 18
30	0.370 – 18	0.474 – 18	0.782 – 18	0.210 – 18	0.165 – 18
40	0.299 – 18	0.256 – 18	0.513 – 18	0.224 – 18	0.196 – 18
50	0.271 – 18	0.190 – 18	0.350 – 18	0.195 – 18	0.155 – 18
60	0.256 – 18	0.180 – 18	0.268 – 18	0.144 – 18	0.117 – 18
70	0.245 – 18	0.187 – 18	0.211 – 18	0.122 – 18	0.978 – 19
80	0.231 – 18	0.201 – 18	0.187 – 18	0.119 – 18	0.886 – 19
90	0.228 – 18	0.223 – 18	0.177 – 18	0.119 – 18	0.795 – 19
100	0.222 – 18	0.237 – 18	0.204 – 18	0.122 – 18	0.768 – 19
110	0.219 – 18	0.244 – 18	0.260 – 18	0.131 – 18	0.731 – 19
120	0.213 – 18	0.245 – 18	0.356 – 18	0.141 – 18	0.704 – 19
130	0.211 – 18	0.240 – 18	0.502 – 18	0.154 – 18	0.685 – 19
140	0.208 – 18	0.233 – 18	0.735 – 18	0.170 – 18	0.667 – 19
150	0.205 – 18	0.224 – 18	0.969 – 18	0.189 – 18	0.649 – 19
160	0.202 – 18	0.213 – 18	0.121 – 17	0.211 – 18	0.631 – 19
170	0.199 – 18	0.202 – 18	0.141 – 17	0.236 – 18	0.612 – 19
180	0.196 – 18	0.190 – 18	0.152 – 17	0.265 – 18	0.594 – 19

the DCS's for the E and a'' states at energies of 20 eV and higher suggests that the difference in the strength of the singlet and triplet coupling of the Rydberg electron to the $N_2^+(X\,^2\Sigma_g^+)$ core is relatively weak compared to other factors affecting the scattering process. This interpretation has a certain intuitive appeal based on the picture of the Rydberg electron as very diffuse, and this type of weak coupling (Ω_c, ω) in Rydberg states has been studied in optical spectroscopy.[35] The DCS's for excitation of the E and a'' states are tabulated in Tables X and XI, respectively.

V. DISCUSSION OF RESULTS

A. Semiclassical interpretation of the DCS's

A simple, semiclassical picture of the electron-impact excitation process can be used as a qualitative explanation of many of the characteristic features of the DCS's for excitation of the singlet, triplet, and Rydberg states of N_2 and perhaps other diatomic molecules.

1. Singlet-singlet excitations

Electron-impact excitation processes in neutral targets between singlet states are associated with interaction potentials of various range,[36] according to whether the transition is allowed by electric-dipole, magnetic-dipole, electric-quadrupole, etc. -type terms. These interactions are of longer range than the exchange interactions and can account for the observed forward peaking in the DCS's as follows. Long-range interactions correspond to large classical impact parameters and therefore small scattering angles. Since a relatively large number of the scattering events occur at large impact parameters, forward scattering will dominate the DCS for singlet-singlet transitions at the higher incident electron energies. Although no dipole-allowed transitions are reported here, DCS's for excitation of three singlet states are presented which demonstrate this characteristic at the higher-impact energies. Both previously published work[36] and work to be reported[20] show this effect for states that are dipole-connected to the ground state.

2. Singlet-triplet excitation

Singlet-triplet (or triplet-singlet) excitation processes in low-Z atoms or diatomic molecules (where l-s coupling dominates) are generally exchange scattering in character in which the incident electron replaces one of the target electrons, which then becomes the scattered electron. The classical picture for this process requires that the incident electron penetrate the electron cloud of the target in order that the exchange of identical particles occur. The range of impact parameters for which this penetration can occur (classically) is relatively small, and therefore DCS's for exchange excitations would be expected to have little or no forward peaking. Figures 14–17 illustrate this characteristic in that none of these DCS's show significant forward peaking. This classical picture

of exchange scattering also allows for a *qualitative* description of the general backward peaking (see Figs. 14–17) of DCS's for the exchange excitation processes. That is, the requirement that the incident electron penetrate the electron cloud of the target means that many of the scattering events will be "direct hits." One can rationalize that the electron-electron repulsion then forces the "scattered" electron back in the same general direction from which the incident electron came.

3. *Excitation of Rydberg and Σ^- states*

The DCS's for excitation of the E and a'' states are strikingly similar, as seen from Figs. 23 and 24. These states are both formed from the ($3\sigma_g \rightarrow 3s\sigma_g$) excitation, for triplet and singlet coupling to the $N_2^+(^2\Sigma_g^+)$ core, respectively. The immediate conclusion to be drawn from the similarity of the DCS's is that the Rydberg electron is only loosely spin-coupled to the N_2^+ core, as pointed out above. The strong forward peaking of the DCS's further suggests (in the classical model) that the transitions are relatively easily induced by long-range interactions. This interpretation is consistent with the view of the Rydberg electron as being diffuse spatially, weakly coupled to the other bound electrons, and consequently highly polarizable.

The DCS's for the $\Sigma^+ \rightarrow \Sigma^-$ transitions do not appear to be easily explained in terms of the classical picture. This may not be particularly surprising because the transition is forbidden in any scattering model based on first-order perturbation theory,[17(a)] and a quantum-mechanical description is necessary in order to explain[34] the behavior of the DCS at 0° and 180° scattering angles.

It is clear that considerably more experimental and theoretical work needs to be done on electron-molecule (atom) scattering before the details of the excitation process can be understood beyond the simple qualitative arguments given above. A detailed theoretical analysis of the DCS's reported here in terms of the inelastic K-matrix elements is presently under way[37] in the hope that more quantitative information about the inelastic-scattering process will result.

B. Comparison with theory

As mentioned above, the only calculations that have been reported in detail for the electron-impact excitation of electronic states in diatomic molecules are those based on first-order scattering theories such as Born or Born-Ochkur-Rudge. The difficult mathematical problems associated with correctly incorporating the non-central-force character of the electron-molecule interaction has, until very recently, limited the theoretical work to these more simplistic theories. (Work is now under way to extend the R-matrix method used recently[38] to describe electron-atom scattering, and to apply distorted-wave type theories,[39] to the case of electron-molecule scattering.) Furthermore, the amount of inelastic DCS data previously available has been so limited that the comparisons[12,17] between theory and experiment were incomplete. In this section, a detailed comparison will be made between the present experimental DCS's and those predicted by the Born-Ochkur-Rudge[12,17,40] theories. No other theoretical results have been reported for the inelastic electron scattering by N_2 for comparison with the present results.

The first theoretical efforts to describe the electronic excitation of simple diatomic molecules[40,41,17(a)] utilized Slater-type orbitals for the target molecular wave functions. Although Slater basis functions are very well suited for bound-state calculations (e.g., proper cusp and asymptotic behavior), the relevant matrix elements that need to be evaluated in Born-type theories cannot be done in general using these basis functions. These matrix elements either need to be approximated for certain values of the momentum transfer[40] or the range of angular momentum coupling needs to be restricted[41,17(a)] to small values. However, the use of Gaussian-type atomic basis functions for the target molecule allows all Born-type scattering integrals to be evaluated in closed form, as was first shown by Miller and Krauss.[42] As a result of these substantial mathematical simplifications, first-order-type scattering theories can now be done almost as quickly for molecules as for atomic targets. The results of Chung and Lin,[17(b)] who employed Gaussian-type atomic basis functions, represent the most extensive application of first-order scattering theories to the excitation of N_2 and will be used for comparison to the present experimental results.

Although Chung and Lin did not specifically provide theoretical DCS results, it is possible to recast their published results, given in terms of the scaled generalized-oscillator-strength (GOS), in terms of DCS's so that direct comparisons can be made to the present results. The relationships between the scaled GOS $[G_{on}(K)]$ and the DCS's is given below, following the notation of Chung and Lin.[17(b)] For excitation of the singlet states in the Born-Ochkur first-order model, the DCS can be expressed in terms of the scaled GOS as (atomic units)

$$\frac{d\sigma^s}{d\Omega}(\theta,\varphi) = \frac{k'}{k}\,\frac{(2k^2-K^2)^2}{2k^2K^2}\,G_{on}(K)\,, \tag{11}$$

where K, the scalar momentum transfer, is given

by

$$K^2 = 2k^2 - \Delta E\, 2k^2 (1 - \Delta E/k^2)^{1/2} \cos\theta \tag{12}$$

and

$$k'/k = (1 - \Delta E/k^2)^{1/2} . \tag{13}$$

In deriving Eq. (11), the DCS for specific vibrational states was summed over all final vibrational states. The most reasonable definition for the quantity ΔE is the weighted-average energy for excitation of a given electronic state; e.g.,

$$\Delta E = \sum_{v'} \Delta E(v')\, q_{v'} , \tag{14}$$

where $q_{v'}$ is the Franck-Condon factor. This is a reasonable approximation when the incident electron energy is sufficiently above threshold ($E \gtrsim 20$ eV), which is also consistent with the foundation of the first-order model. The scaled GOS, $G_{on}(K)$, differs from the usual definition of the GOS, $f_{on}(K)$, in that the defining equation[17(b)] does not contain the excitation energy for the transition; i.e.,

$$f_{on}(K) = (\Delta E)\, G_{on}(K) . \tag{15}$$

This definition was chosen so that a quantity could be obtained that depended only on the Fourier transform of the transition charge density (not on the energies of the approximate wave functions) and so that the sensitivity of the results on variations in the approximate wave functions could be isolated.

Figure 25 compares the DCS for excitation of the $a\,^1\Pi_g$ state, obtained in the Born-Ochkur model [using the $G_{on}(K)$ values from Ref. 17(b) and Eqs. (11)–(14)] with the present results obtained from experimental data, for incident electron energies of 20 and 50 eV. The results in Fig. 25 show that the DCS's predicted by the Born-Ochkur model are accurate to about a factor of 2 in the angular range 0° to about 20° and are qualitatively accurate out to about 60°. For larger scattering angles, the Born-Ochkur results agree poorly with the measured DCS's. In addition, the Born-Ochkur DCS's have a node at intermediate scattering angles that is "artificially" introduced by the scattering model,[36,43] which renders the theoretical DCS's useless for scattering angles greater than about 60°.

Theoretical DCS's for excitation of the triplet states of N_2 can also be obtained from the scaled GOS results of Chung and Lin.[17(b)] For these exchange excitation processes, they employed the Ochkur-Rudge approximation for which

$$\frac{d\sigma^T}{d\Omega}(\theta, \varphi) = \frac{3k'}{2k} \frac{K^2}{(k'^2 + \epsilon)^2} G_{on}(K) , \tag{16}$$

where ϵ is the N_2 ionization energy (in Ry) and the other symbols have the same meaning as in Eqs. (11)–(14). Figures 26–29 show comparisons of theoretical and measured DCS's for excitation of the $A\,^3\Sigma_u^+$, $W\,^3\Delta_u$, $C\,^3\Pi_u$, and $E\,^3\Sigma_g^+$ states, respectively, at 20- and 50-eV incident electron energy. In all cases, the theoretical DCS could not be obtained for *all* scattering angles at 50 eV because

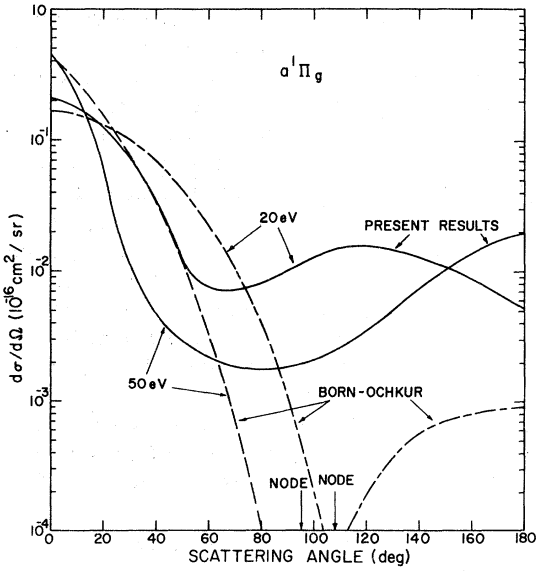

FIG. 25. Comparison of the DCS's for excitation of the a state obtained from the present study with those predicted by the Born-Ochkur model for incident electron energies of 20 and 50 eV. See text for discussion.

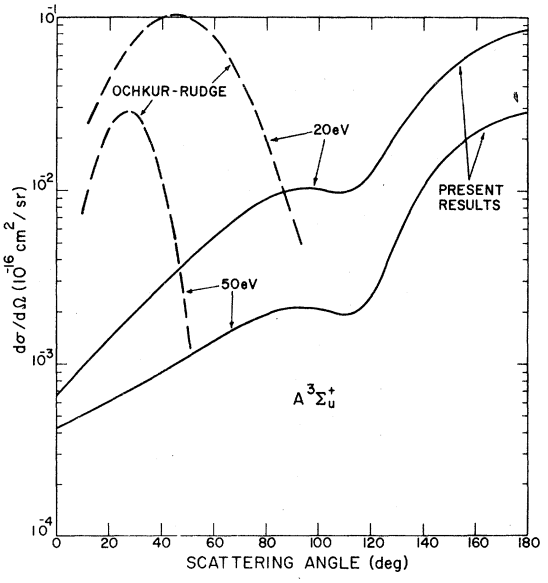

FIG. 26. Comparison of the DCS's for excitation of the A state obtained from the present study with those predicted by the Ochkur-Rudge model, for incident electron energies of 20 and 50 eV. See text for discussion.

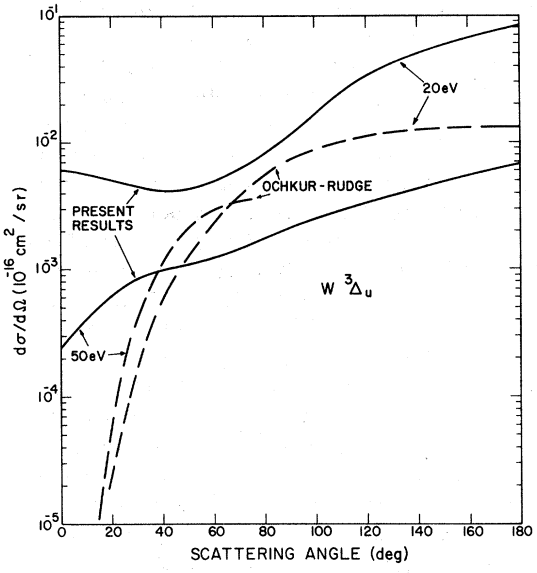

FIG. 27. Same as Fig. 26, but for excitation of the W state. See text for further discussion.

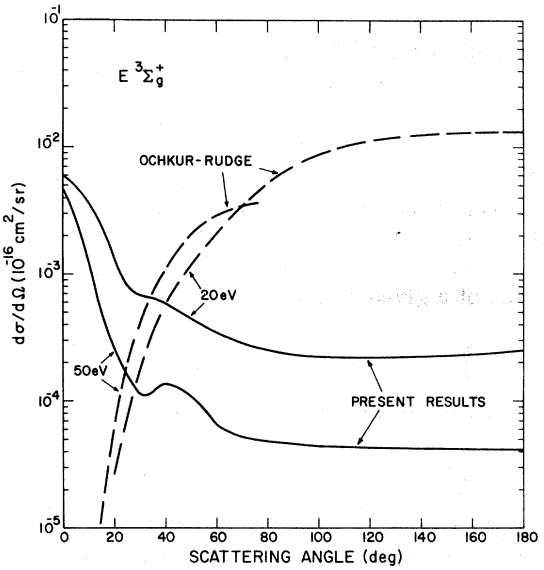

FIG. 29. Same as Figs. 26–28, but for excitation of the E state. See text for further discussion.

$G_{on}(K)$ had not been calculated for sufficiently large values of K. These figures show that, in all cases, the theoretical DCS's are not even in qualitative agreement with those measured. Furthermore, in some cases (e.g., A and C states), the agreement is poorer at 50 eV than at 20 eV. This fact is surprising because the Ochkur-Rudge model is based on a high-energy approximation so that the agreement should improve, or at least not worsen, as the incident electron energy increases. Comparison at higher incident electron energy could not be done because the present measurements did not extend beyond 50 eV.

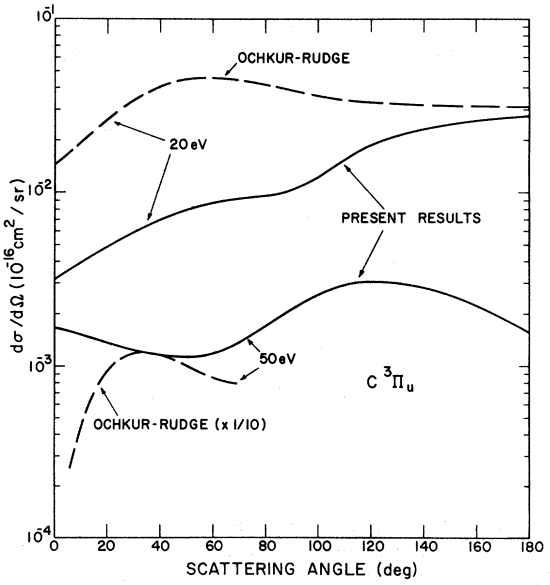

FIG. 28. Same as Figs. 26 and 27, but for excitation of the C state. See text for further discussion.

Although it was suggested earlier[12,18] that agreement frequently obtained when using *integral* Born-Ochkur and Ochkur-Rudge models may only be fortuitous, the comparison between theory and experiment shown in Figs. 26–29 is a great deal poorer than expected. Previous comparisons[43,44] between first-order theories and experiment have shown the angular and energy regions of validity depend a great deal on the symmetries of the initial and final target states. Of the various theoretical DCS's considered here, only those for excitation of the $a\,^1\Pi_g$ state show some resemblance to the experimental results and then only out to about 30° scattering angle. The reason why first-order exchange theories do so poorly in describing the DCS's for excitation of the N_2 triplet states, even at 50-eV incident electron energy, is not clear. The comparisons presented here indicate that further theoretical work is needed on first-order exchange theories to learn more about the range of validity of the scattering model. This is particularly important for the excitation of Rydberg states and the variations in the theoretical DCS's as a function of the incident electron energy.

C. DCS's as a function of energy and angle

Figure 30 is a composite of perspective plots for five different DCS's and illustrates the kind of variation that occurs, as a function of both incident electron energy and scattering angle, de-

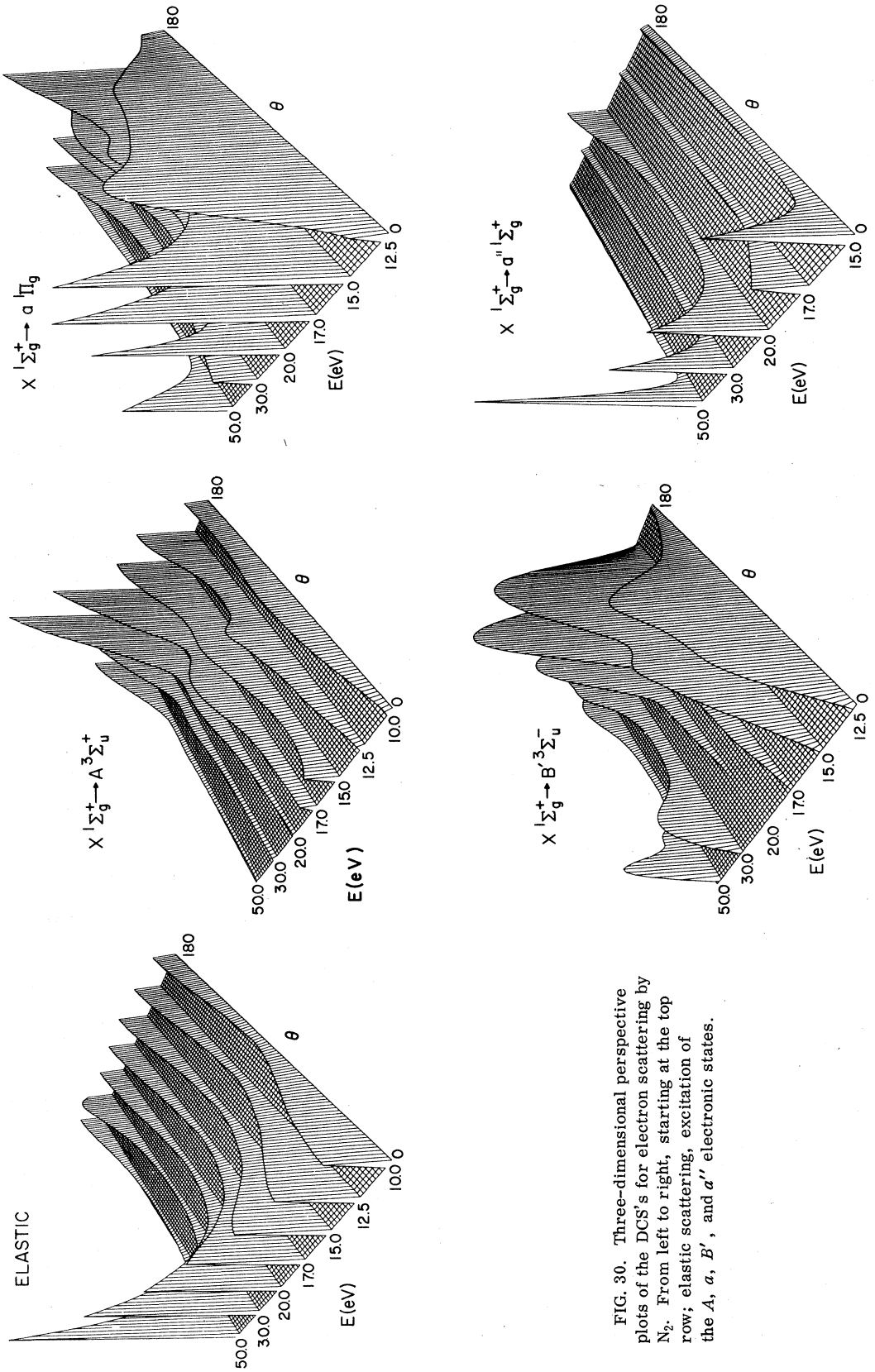

FIG. 30. Three-dimensional perspective plots of the DCS's for electron scattering by N_2. From left to right, starting at the top row; elastic scattering, excitation of the A, a, B', and a'' electronic states.

pending on whether the scattering process is elastic or inelastic with pure exchange or direct plus exchange.

The forward or backward peaking and the rapid energy variation of the DCS's for the inelastic processes are evident from this type of figure. Perspective figures of the other DCS's discussed here, as well as for nine electronic states between 12.5 and 14.2 eV, will be presented in a monograph[32] along with all the data used in this study.

ACKNOWLEDGMENTS

This work would not have been completed without the excellent technical assistance of G. R. Steffensen (Jet Propulsion Laboratory) in building the electron spectrometers and of N. A. Fiamengo (Aerospace Corporation) in helping develop the computational techniques necessary to analyze the data. The authors thank S. Chung and C. C. Lin for sending us the tabulated results of their calculations.

---

‡Work supported in part by the USAF SAMSO Contract No. F04701-75-C-0076; the U.S. Energy Research and Development Administration to Los Alamos; and NASA, Contract No. NAS7-100 to Jet Propulsion Laboratory.

*Present address.

[1]S. K. Srivastava, A. Chutjian, and S. Trajmar, J. Chem. Phys. 64, 1340 (1976).

[2]J. F. Williams, J. Phys. B 9, 1519 (1976).

[3]A. E. Kingston, W. C. Fon, and P. G. Burke, J. Phys. B 9, 605 (1976).

[4]S. Trajmar, Phys. Rev. A 8, 191 (1973); A. Yagishita, T. Takayanagi, and H. Suzuki, J. Phys. B 9, L53 (1976); A. Chutjian and S. K. Srivastava, J. Phys. 8, 2360 (1975), and references therein.

[5]A. Chutjian and L. D. Thomas, Phys. Rev. A 11, 1583 (1975); A. Chutjian, J. Phys. B 9, 1749 (1976).

[6]A. L. Sinfailam, J. Phys. 9, L101 (1976).

[7]W. Williams and S. Trajmar, Phys. Rev. Lett. 33, 187 (1974).

[8]W. Williams and D. Bozinis, Phys. Rev. A 12, 57 (1975).

[9]W. Williams, S. Trajmar, and D. G. Bozinis, J. Phys. B 8, L96 (1975).

[10]W. Williams and S. Trajmar, J. Phys. B 8, L50 (1975).

[11]N. W. Winter, D. C. Cartwright, and M. M. Wray, in *Electronic and Atomic Collisions, Abstracts of Papers, on the Ninth ICPEAC*, edited by J. S. Riley and R. Geballe (University of Washington Press, Seattle, 1975), Vol. 2, p. 1023.

[12]S. Trajmar, D. C. Cartwright, J. K. Rice, R. T. Brinkmann, and A. Kuppermann, J. Chem. Phys. 49, 5464 (1968).

[13]S. Trajmar, D. C. Cartwright, and W. Williams, Phys. Rev. A 4, 1482 (1971).

[14]F. Linder and H. Schmidt, Z. Naturforsch. 26a, 1617 (1971).

[15]T. G. Finn and J. P. Doering, J. Chem. Phys. 64, 4490 (1976).

[16]E. N. Lassettre and A. Skerbele, in *Methods of Experimental Physics* (Academic, New York, 1974), Vol. 3, p. 868, and references therein.

[17](a) D. C. Cartwright, Phys. Rev. A 2, 1331 (1970); *ibid.* 5, 1974 (1972); (b) S. Chung and C. C. Lin, Phys. Rev. A 6, 988 (1972).

[18]P. S. Julienne and M. Krauss, J. Res. Natl. Bur. Stand. (U.S.) A, 76, 661 (1972).

[19]D. C. Cartwright, S. Trajmar, A. Chutjian, and W. Williams, Phys. Rev. 16, 1041 (1977) (first following paper).

[20]A. Chutjian, D. C. Cartwright, and S. Trajmar, Phys. Rev. A 16, 1052 (1977) (second following paper).

[21]S. Trajmar, J. K. Rice, and A. Kuppermann, *Advances in Chemical Physics*, (Wiley, New York, 1970), Vol. 18.

[22]A. Chutjian, D. C. Cartwright, and S. Trajmar, Phys. Rev. Lett. 30, 195 (1973).

[23]A. Chutjian, J. Chem. Phys. 61, 4279 (1974).

[24]S. Trajmar, Phys. Rev. A 8, 191 (1973).

[25]R. I. Hall, G. Joyez, J. Mazeau, J. Reinhardt, and G. Schermann, J. Phys. (Paris) 34, 827 (1973); F. H. Read, J. Phys. B 8, 1034 (1975).

[26](a) Obtained by using modified versions of the original RKR and Franck-Condon programs written by R. N. Zare, UCRL Report No. 10925, 1963 (unpublished). (b) See also D. E. Albritton, A. Schmeltekopf, and R. N. Zare, *Diatomic Intensity Factors*, (Harper and Row, New York, 1976).

[27]W. Benesch, J. T. Vanderslice, S. G. Tilford, and P. G. Wilkinson, Astrophy. J. 142, 1227 (1965).

[28]R. Covey, K. A. Saum, and W. M. Benesch, J. Opt. Soc. Am. 63, 592 (1973).

[29]Y. Tanaka, M. Ogawa, and A. S. Jursa, J. Chem. Phys. 40, 3690 (1964).

[30]J. W. Ledbetter, J. Mol. Spectrosc. 42, 100 (1972).

[31]D. C. Cartwright, N. A. Fiamengo, and J. K. Rice (unpublished).

[32]D. C. Cartwright, S. Trajmar, A. Chutjian, and W. Williams, Los Alamos Monograph Series, University of California (to be published).

[33]J. Mazeau, F. Gresteau, R. I. Hall, G. Joyez, and J. Reinhardt, J. Phys. B 6, 862 (1973).

[34]D. C. Cartwright, S. Trajmar, W. Williams, and D. L. Huestis, Phys. Rev. Lett. 27, 704 (1971); W. A. Goddard, D. L. Huestis, D. C. Cartwright, and S. Trajmar, Chem. Phys. Lett. 11, 329 (1971).

[35]G. Herzberg, *Molecular Spectra and Molecular Structure: I. Spectra of Diatomic Molecules*, 2nd ed., (Van Nostrand, New York, 1950), p. 338.

[36]D. G. Truhlar, J. K. Rice, S. Trajmar, and D. C. Cartwright, Chem. Phys. Lett. 9, 299 (1971).

[37]D. C. Cartwright (to be published).

[38]B. I. Schneider, M. A. Morrison, and P. J. Hay, Bull. Am. Phys. Soc. 21, 1257 (1976), (EB-8).

[39]T. N. Rescigno, C. W. McCurdy, and B. W. McKoy (to be published).

[40]B. F. Rozsnyai, J. Chem. Phys. 47, 4102 (1967).

[41]D. C. Cartwright and A. Kuppermann, Phys. Rev. 163, 86 (1967).

[42]K. J. Miller and M. Krauss, J. Chem. Phys. 47, 3754 (1967).
[43]D. G. Truhlar, J. K. Rice, A. Kuppermann, S. Trajmar, and D. C. Cartwright, Phys. Rev. A 1, 778 (1970).
[44]Y. K. Kim and M. Inokuti, Phys. Rev. 175, 176 (1968); L. Vriens, J. A. Simpson, and S. R. Mielczarek, J. Chem. Phys. 165, 7 (1968); J. K. Rice, D. G. Truhlar, D. C. Cartwright, and S. Trajmar, Phys. Rev. A 5, 762 (1972).